atmosphere

MDPI

Article

Non-Hydrostatic Regcm4 (Regcm4-NH): Evaluation of Precipitation Statistics at the Convection-Permitting Scale over Different Domains

Paolo Stocchi [1,*], Emanuela Pichelli [2], Jose Abraham Torres Alavez [3], Erika Coppola [2], Graziano Giuliani [2] and Filippo Giorgi [2]

[1] National Research Council of Italy, Institute of Atmospheric Sciences and Climate, CNR-ISAC, 40129 Bologna, Italy

[2] International Centre for Theoretical Physics, Earth System Physics (ICTP-ESP), 34014 Trieste, Italy; epichell@ictp.it (E.P.); coppolae@ictp.it (E.C.); ggiulian@ictp.it (G.G.); giorgi@ictp.it (F.G.)

[3] Institute for Atmospheric and Climate Science, ETH-Zurich, 8000 Zurich, Switzerland; abraham.torres@env.ethz.ch

* Correspondence: p.stocchi@isac.cnr.it

Citation: Stocchi, P.; Pichelli, E.; Torres Alavez, J.A.; Coppola, E.; Giuliani, G.; Giorgi, F. Non-Hydrostatic Regcm4 (Regcm4-NH): Evaluation of Precipitation Statistics at the Convection-Permitting Scale over Different Domains. *Atmosphere* **2022**, *13*, 861. https://doi.org/10.3390/atmos13060861

Academic Editor: Stefan Liess

Received: 6 May 2022
Accepted: 19 May 2022
Published: 25 May 2022

Abstract: Recent studies over different geographical regions of the world have proven that regional climate models at the convection-permitting scale (CPMs) improve the simulation of precipitation in many aspects, such as the diurnal cycle, precipitation frequency, intensity, and extremes at daily—but even more at hourly—time scales. Here, we present an evaluation of climate simulations with the newly developed RegCM4-NH model run at the convection-permitting scale (CP-RegCM4-NH) for a decade-long period, over three domains covering a large European area. The simulations use a horizontal grid spacing of ~3 km and are driven by the ERA-Interim reanalysis through an intermediate driving RegCM4-NH simulation at ~12 km grid spacing with parameterized deep convection. The km-scale simulations are evaluated against a suite of hourly observation datasets with high spatial resolutions and are compared to the coarse-resolution driving simulation in order to assess improvements in precipitation from the seasonal to hourly scale. The results show that CP-RegCM4-NH produces a more realistic representation of precipitation than the coarse-resolution simulation over all domains. The most significant improvements were found for intensity, heavy precipitation, and precipitation frequency, both on daily and hourly time scales in all seasons. In general, CP-RegCM4-NH tends to correctly produce more intense precipitation and to reduce the frequency of events compared to the coarse-resolution one. On the daily scale, improvements in CP simulations are highly region dependent, with the best results over Italy, France, and Germany, and the largest biases over Switzerland, the Carpathians, and Greece, especially during the summer seasons. At the hourly scale, the improvement in CP simulations for precipitation intensity and spatial distribution is clearer than at the daily timescale. In addition, the representation of extreme events is clearly improved by CP-RegCM4-NH, particularly at the hourly time scale, although an overestimation over some subregions can be found. Although biases between the model simulations at the km-scale and observations still exist, this first application of CP-RegCM4-NH at high spatial resolution indicates a clear benefit of convection-permitting simulations and encourages further assessments of the added value of km-scale model configurations for regional climate change projections.

Keywords: regional climate models; RegCM4; km-scale resolution; Mediterranean; Europe; convection permitting; extreme precipitation

1. Introduction

Over the past decade, computational advances and updates of Regional Climate Model (RCM) systems to non-hydrostatic frameworks has allowed the application of RCMs to continuous long-term simulations at very high resolutions, the so-called "convection-permitting" (CP) scale, i.e., with kilometer-scale grid spacing (order of 1–4 km) [1–8]. These models, which we refer to as Convection-Permitting Regional Climate Models (CP-RCMs), allow the explicit representation of deep convective processes without the use of parameterization schemes [1,3,9]. Indeed, the parametrization of convection in standard RCMs is considered to be a major source of model errors and uncertainty [10,11]. In particular, most models relying on convection schemes show deficiencies in simulating the diurnal cycle of precipitation, tend to underestimate the intensity and overestimate the frequency of sub-daily precipitation, fail to simulate mesoscale convective systems, and lack the ability to advect diagnosed convection or trigger new showers along convective outflow boundaries [12–15].

CP-RCMs can provide a step change in our understanding of future changes at local scales and in the simulation of extreme weather events [16–20], although there are still key challenges to address. For example, CP-RCMs tend to produce overly intense precipitation and have issues in representing land-surface processes; in addition, sub-kilometer-scale processes other than convection still need to be parametrized, with existing parameterization schemes often requiring development for use at such scales. Within this framework, the use of CP-RCMs requires substantial assessment and evaluation for climate applications.

While the use of CP-RCMs has been consolidated in short-range regional weather forecasting for almost two decades [21–31], the application within the context of long-term climate simulations is relatively new. Until recently, due to the high computational cost of running CP-RCMs, long-term simulations at convection-permitting resolutions have been limited to typically small regional domains, e.g., UK [3,4,32,33], Germany and Central Europe [34,35], France [8,36], Iberian Peninsula [37], the Alps [2,38–41], Scandinavia [42], and Belgium [43]. Few studies have been carried out over whole continental domains, e.g., the continental U.S. [6], Europe [5,7,44], and Africa [45,46]. These studies have shown that CP-RCMs do provide an important added value (AV) in the simulation of regional and local climate processes, for example, improving the representation of hourly rainfall characteristics [2,3,40], such as intensity, frequency, and extremes along with the diurnal cycle of convection [32,42].

Studies focusing on future changes in precipitation show that future increases in short-duration precipitation extremes are larger in CP-RCMs compared to coarser-resolution counterparts [6,47], with evidence in some regions of super Clausius–Clapeyron scaling for extreme hourly precipitation intensities [44,48,49]

Recently, CP-RCMs inter-comparison projects such as the CORDEX Flagship Pilot Study on convection (CORDEX-FPS) [41,50,51]), the European Climate Prediction System (EUCP) [52], and the first ensemble of CP-RCM projections for the UK Climate Projections project (UKCP [53]) have enabled the first multi-model and multi-scale assessments of precipitation extremes, going from coarser convection-parameterized models down to CP-RCMs. These studies showed that CP-RCMs may lead to a significant reduction of model uncertainties, particularly concerning the projection of extreme rainfall events and the structure and evolution of mesoscale convective systems [53–57]. This is of high importance, e.g., for the assessment of changes in severe natural hazards, such as flash floods affecting urban areas and small river catchments [47,58].

The need to produce climate information at local scales will bring about increasing demand for climate models able to work at the CP scale, which will require much effort in assessing model performance. In fact, the use of CP-RCMs for climate applications is not a simple resolution refinement of hydrostatic models; it is a truly qualitative step requiring substantial model developments, not only in the implementation of non-hydrostatic dynamical cores, but also in the representation of physical processes such as cloud and precipitation microphysics.

Within this general research framework, recently, a non-hydrostatic version of the regional climate model RegCM4 [59] was developed, called RegCM4-NH [60]. The model was used to produce decade-long simulations at convection-permitting scales over three

European subdomains in the framework of two international CP-RCM inter-comparison projects: the CORDEX-FPS on convection simulation [51] and the European Climate Prediction System (EUCP) [52]. The three domains simulated with CP-RegCM4-NH included the so-called greater Alpine region (AL), South-East Europe (SE), and Central East Europe (CE) (Figure 1).

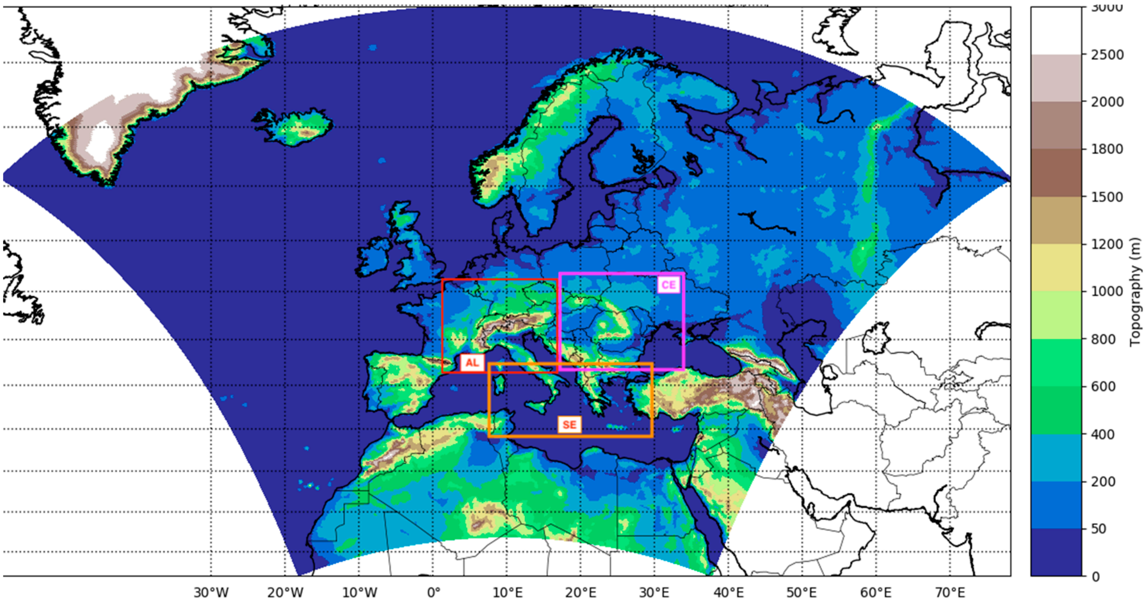

Figure 1. Set of domains simulated by CP-RegCM4-NH (3 km grid size) in EUCP project nested into EUR11 domain, simulated by RegCM4-NH (12 km grid size). The Alps (AL), red box; Central East Europe (CE), purple box; South East Europe (SE), orange box.

The aim of this work is to present an initial validation of these CP simulations, focusing on different precipitation statistics produced with the model driven by the ERA-Interim reanalysis of observations through an intermediate run (RegCM4-NH) at a coarser resolution (12 km). We compare the CP-RegCM4-NH (3 km) simulations against available high-resolution observations (Table 1) and the RegCM4-NH (12 km) driving run. We analyse both daily and sub-daily precipitation statistics, focusing on the benefits and limitations of running RegCM4-NH at the kilometer scale over climate timescales. The main aim of our analysis is to identify the added value of running CP-RegCM4-Nh compared to the coarser-resolution driving counterpart.

The structure of this manuscript is as follows: Section 2 presents the data and methodology of this study, Section 3 discusses results on the evaluation of precipitation characteristics, and Section 4 presents final considerations.

2. Data and Methods

2.1. Methods

We focus our analysis on a number of statistical indices detailed in Table 2: Seasonal mean daily precipitation, seasonal wet-day/hour intensity, seasonal wet-day/hour frequency, seasonal heavy precipitation (defined as the 99th and 99.9th percentile of all daily and hourly precipitation events, respectively). We further evaluate the model performance using the probability distribution of precipitation intensities, the relative bias, the spatial variability, and correlation.

The indices are calculated as seasonal values for summer, June–July–August; winter, December–January–February; spring, March–April–May; and autumn, September–October–November. For all indices, models and observational data are kept on their original grid to retain as detailed a representation as possible. However, as the calculation of metrics such as the relative bias, spatial correlation, and spatial variability requires a grid-by-grid comparison between model and observations, for these cases, the observational and model data were remapped onto a common 3 km grid for the evaluation of the CP-RegCM4-NH runs, and to the ~12 km EURO-CORDEX grid for the RegCM4-NH simulations.

2.2. Model Simulations

Here, we investigate the CP-RegCM4-NH [60] simulations at 3 km grid spacing over the three subdomains shown in Figure 1: the Alps (AL), South-East Europe (SE), and Central Europe (CE). Fields from the ERA-Interim reanalysis [61] are used to provide initial and lateral boundary atmospheric conditions for the intermediate resolution run of RegCM4-NH at 12 km grid spacing over a domain covering the entire European region; this, in turn, provides initial and lateral boundary conditions for the convection-permitting experiments with CP-RegCM4-NH at 3 km (updated every 6 h). No domain-side nudging to the ERA-Interim driven data or other data sources has been used. The new RegCM-NH core [60] allows for acoustic wave damping and Rayleigh damping at the top model levels, which can be used to make the model solution more stable by controlling mechanical wave amplification (see Refs. [60,62] for details).

The RegCM4-NH run uses a parameterization of deep convection [59], while in the CP-RegCM4-NH, convection is explicitly resolved and only a trigger for shallow convection remains. All simulations share the non-hydrostatic dynamical core [60]. RegCM4-NH uses the following physics schemes: UW-PBL scheme [63], Tiedtke Cumulus convection scheme [64–66], Subex moisture scheme [67], CCSM radiation scheme [68], CLM4.5 Land surface [69], and Zeng Ocean Flux scheme [70]. CP-RegCM4-NH uses the same schemes except for Holstag PBL scheme [71]); the deep cumulus convection is switched off, but a simplified Tiedtke Cumulus scheme is used for triggering non-precipitating shallow convection, with a WSM5 scheme for microphysics [72].

Both for RegCM4-NH and CP-RegCM4-NH, this choice of schemes was found to be the best performing in a series of preliminary tests. The simulation (and evaluation) period is 10 years long (2000–2009) for all domains, following the EUCP and CORDEX-FPS protocols [51]. While longer simulation periods might have provided more robust results, limitations in computing resources led to this choice in the aforementioned projects.

2.3. Observations

A key issue concerning the evaluation of CP-RCMs in many world regions is the availability of high-resolution and high-quality observation datasets. Precipitation measurements essentially come from three distinct sources: In situ rain gauges, ground radars, and satellites. In the present study, we use nine observation datasets described in Table 1. Five of these datasets (EURO4M (alpine region), RdisaggH (Switzerland), COMEPHORE (France), GRIPHO (Italy), and RADKLIM (Germany)) are station based, and provide daily/hourly records representing the highest spatial and temporal resolution data available for the respective subregions (Figure 2). The other four datasets are HMR, PERSIANN-CCS, CHIRPS, and CMORPH, where HMR is a reanalysis dataset, CMORPH and PERSIAN-CCS are based on satellite measurements, and CHIRPS blends satellite imagery with in situ station data (Table 1).

Table 1. The main characteristics of the observational datasets used in the study.

Dataset Name	Available Period	Spatial Res.	Temporal Res.	Data Source	Region	Reference
EURO4M-APGD	1971–2008	5 km	Daily	Station	Alpine region	[73]
RdisaggH	2003–2010	1 km	Hourly	Station + Radar	Switzerland	[74]
COMEPHORE	1997–2016	1 km	Hourly	Station + Radar	France	[8,75]
GRIPHO	2001–2016	3 km	Hourly	Station	Italy	[76]
RADKLIM	2001–2018	1 km	Hourly	Radar + station	Germany	[77]
HMR	1979–2013	5.5 km	Daily	Reanalysis	Europe	[78]
PERSIANN-CCS	2003–present	4 km	Hourly/daily	Satellite	Global	[79]
CHIRPS	1981–present	5.5 km	Daily	Station + Satellite	Global	[80]
CMORPH	2002–present	8 km	30 min	Satellite	Global	[81]

Table 2. Statistical indices analysed in this study (a wet day (hour) is a day (hour) with precipitation ≥ 1 mm (≥ 0.1 mm)).

Index	Definition	Unit
Mean	Mean daily precipitation	mm/day
Frequency	Wet day/hour frequency (defined as fraction of number of wet days/hours per season)	(raction)
Intensity	Wet day/hour intensity	mm/d-mm/h
Heavy Precipitation (p99, p99.9)	99th (99.9th) percentile of all daily/hourly precipitation events (wet and dry)	mm/d-mm/h
Probability density Func. (PDF)	Normalized frequency of occurrence of precipitation events within a certain bin	
Relative Bias	The relative difference $\left(\frac{model-observation}{observation}\right)$ of spatially averaged values for a selected region/domain	
Spatial variability	Ratio $\left(\frac{model}{observation}\right)$ of spatial standard deviations of seasonal values across all grid points of a selected region	
Spatial correlation	The spatial correlation of seasonal values between model and observations across all grid points of a selected region	

When dealing with observations, one should consider shortcomings associated with the types of sensor considered. For example, uncertainties for in situ data are mostly related to low station density (especially over mountainous regions), choice of gridding technique (which can induce underestimation of high intensities trough interpolation), and underestimation of precipitation (due to the problem of gauge undercatch in windy conditions) [82]. Concerning radar measurements, there are mask effect problems in high-altitude terrain areas, while in the case of satellite data, the measurements can be affected by large uncertainties introduced by the physical limitations of the different measurement techniques and the algorithms used to retrieve precipitation from interferometry data [83–86].

For these reasons, different datasets can have significantly different climatologies, especially in areas with low data availability. For example, Ref. [82] analysed seven regional high-resolution datasets, two gauge-based European-wide datasets, and seven global low-resolution ones, showing a substantial spread between different products, often comparable with the spread of model ensembles.

Figures 3–5 show a comparison among the datasets described in Table 1 for some of the indexes described in Table 2: seasonal mean daily precipitation (Figure 3), seasonal daily intensity (Figure 4), and seasonal heavy precipitation, expressed as the 99th percentile of daily precipitation (p99 in Figure 5). The data are presented only for the autumn SON (September–October–November) and summer JJA (June–July–August) seasons, since convective and heavy precipitation events (HPEs) dominate during these seasons over the regions of interest.

The analysis indicates that HMR and the in situ station-based datasets show very similar patterns for mean (Figure 3), intensity (Figure 4), and heavy precipitation (Figure 5), capturing similar spatial details and intensity of extremes. The CMORPH dataset shows particularly low daily mean precipitation in the colder months (Figure 3), while PERSIANN-CCS shows lower precipitation in JJA (Figure 3) and an extremely reduced spatial variability across the domain compared to the other datasets (Figures 4 and 5). The CHIRPS dataset shows patterns for seasonal mean precipitation generally in line with the HMR and in situ ones, along with extremely high precipitation intensities compared to all other datasets (Figure 4).

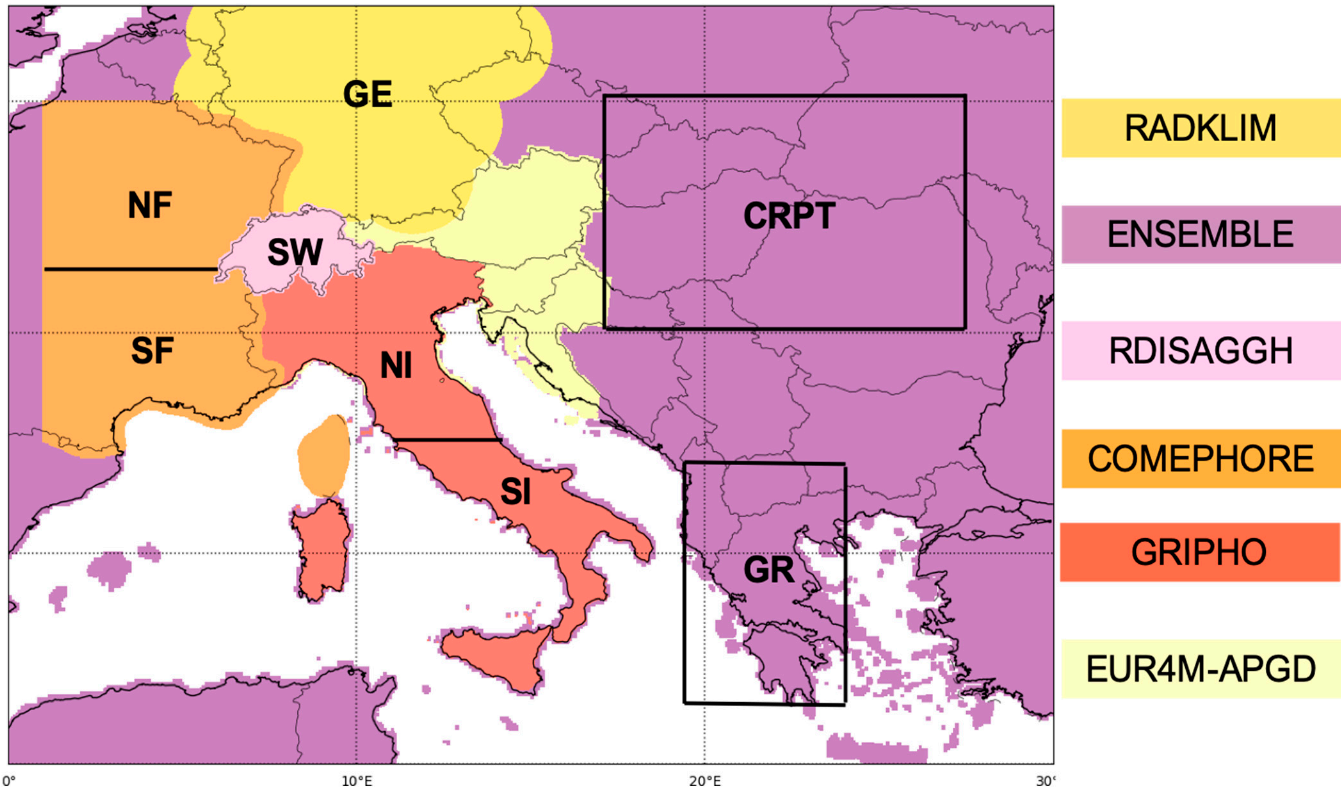

Figure 2. Observational dataset map used for the analysis. EURO4M-APGD (light pastel yellow), GRIPHO (light pastel red), COMEPHORE (orange), RdisaggH (pink), RADKLIM (yellow) and an Ensemble mean of HMR, PERSIANN-CCS, CHIRPS, and CMORPH (purple). EURO4M-APGD and ENSEMBLE are at a daily time scale, while the other datasets are at an hourly time scale. Domains used as evaluation target grids in the PDF analysis are labelled as follows: North and South France (NF, SF), North and South Italy (NI, SI), Switzerland (SW), Germany (GE), the Carpathians (CRPT), and Greece (GR).

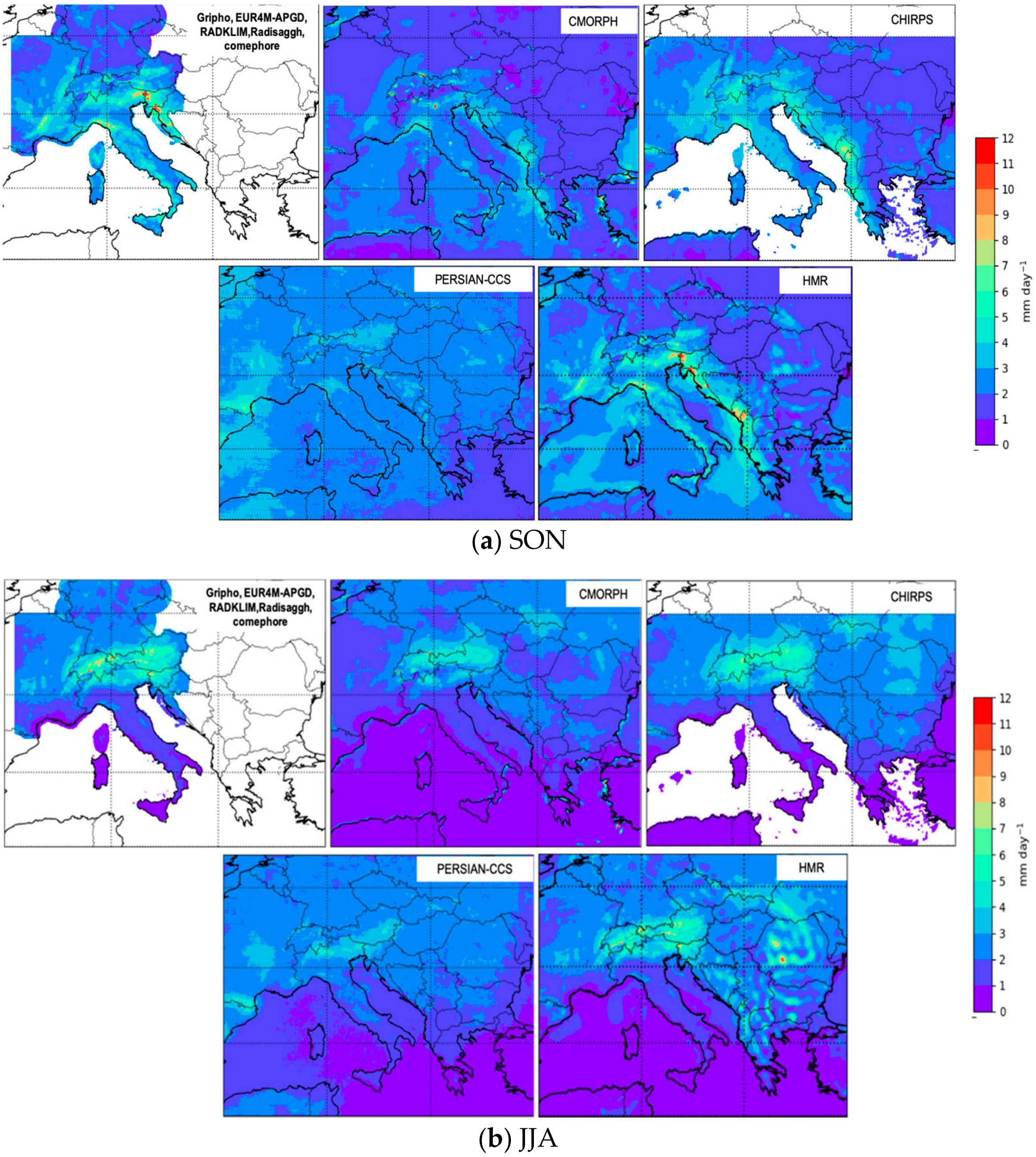

Figure 3. Seasonal mean daily precipitation calculated for different observational datasets described in Table 2 for autumn (**a**) and summer (**b**) seasons.

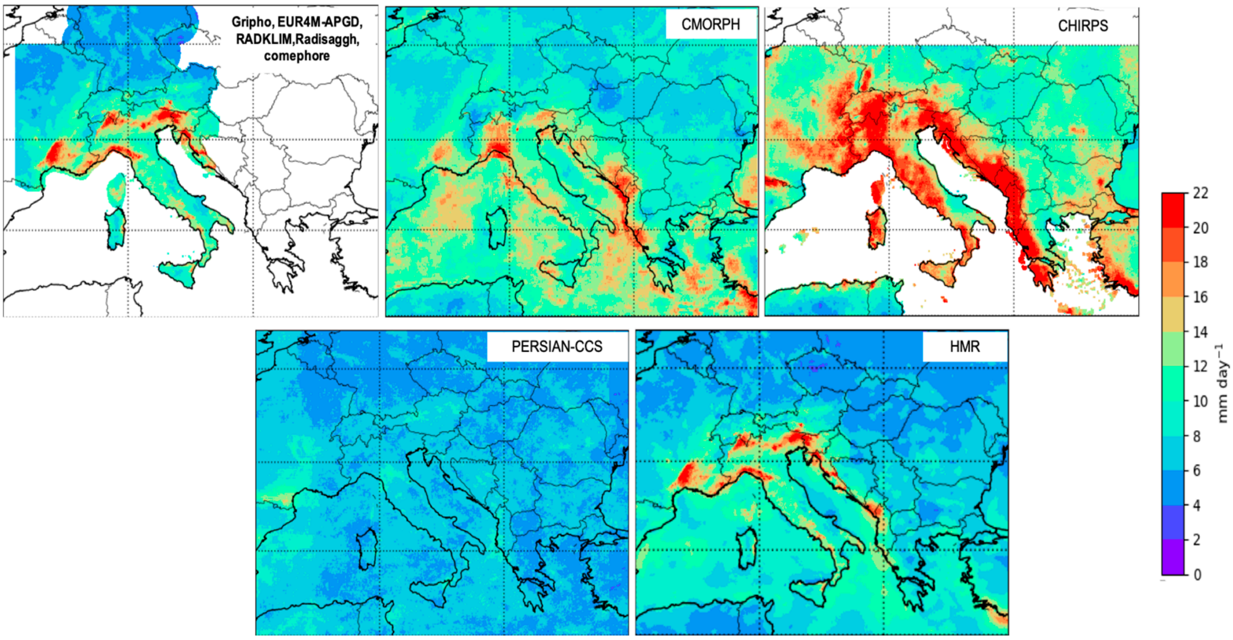

(**a**) SON

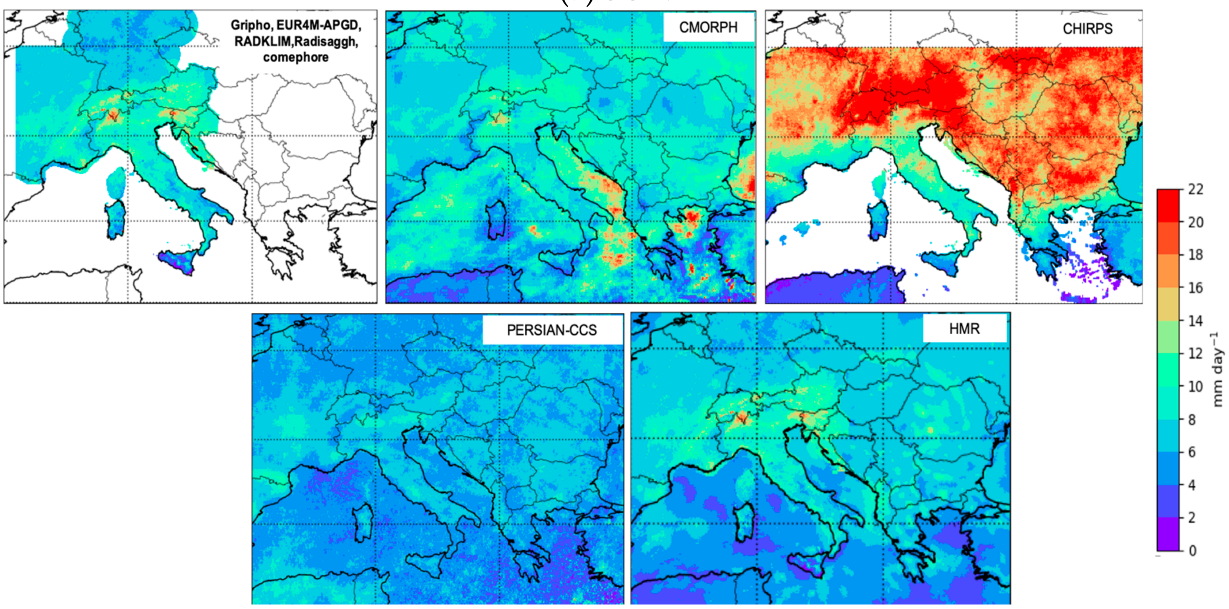

(**b**) JJA

Figure 4. Similar to Figure 3 but for wet-day precipitation intensity.

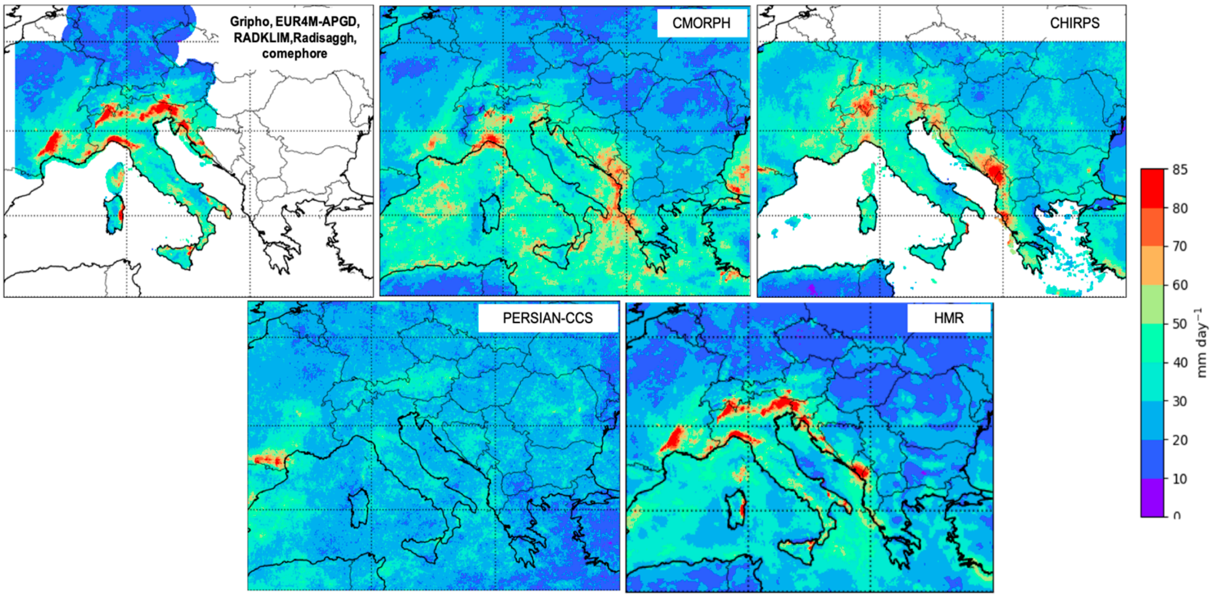

(**a**) SON

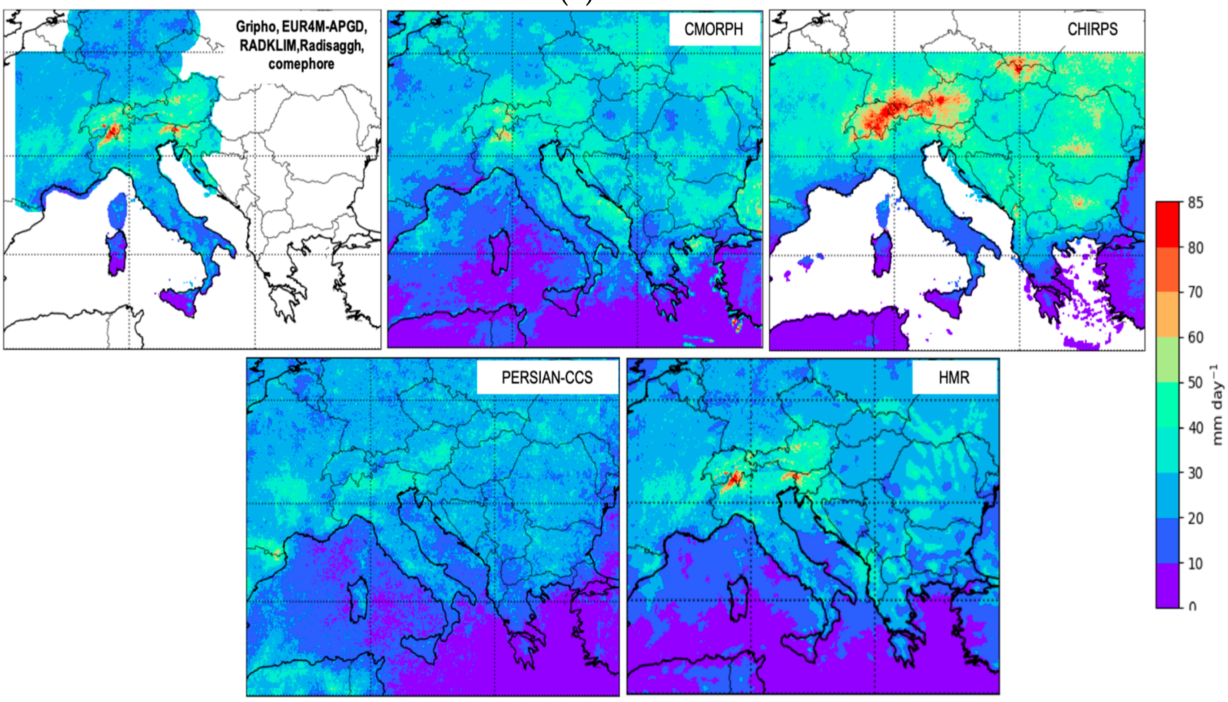

(**b**) JJA

Figure 5. Similar to Figure 3 but for p99.

The comparison among the datasets described in Table 1 confirms that the uncertainty associated with precipitation observations can be large, especially when dealing with precipitation extremes. The satellite-based products (CMORPH, PERSIANN-CCS, and CHIRPS) show large differences compared to high-resolution products, suggesting that they are not sufficiently accurate to validate the model over these regions.

However, it is generally agreed [82,87–89] that in regions where in situ data are available, station-based datasets provide more reliable data. For this reason, where possible, we use only in situ data available for comparison with the model. Specifically, we use the EURO4M (alpine region), RdisaggH (Switzerland), COMEPHORE (France), GRIPHO (Italy), and RADKLIM (Germany) datasets to validate the model over the Alpine domain and an ensemble mean of CMORPH, PERSIANN-CCS, CHIRPS, and HMR for the central and southeastern Mediterranean regions (Figure 2), where, unfortunately, there is lack of in situ high-resolution station observation data. In this regard, the use of ensemble means of observations should reduce related uncertainties [82].

One problem to consider in mountainous areas is the underestimation of precipitation due to the rain gauge undercatch, which is difficult to quantify; it can severely impact the estimate of precipitation, especially for solid precipitation on windy days. According to some studies, this underestimation of total precipitation can be as high as 30–40% for some winter stations [73,90,91], with peaks of 80% in some cases [92]. To account at least partially for these uncertainties, we consider precipitation biases between −5 and +25 to be an acceptable range in some of our analyses.

Finally, for consistency, in our model assessment, we only use periods in which model simulations and corresponding observations overlap, i.e., 2000–2008 for the APGD data; 2003–2010 for the RdissagH; 2000–2009 for GRIPHO; 2000–2009 for COMEPHORE; 2001–2009 for RADKLIM; 2003–2009 for PERSIANN-CCS; and 2000–2009 for HMR, CHIRPS, and CMORPH. Each dataset has been considered over the entire simulation period (2000–2009) if available, or the maximum possible overlapping subperiod. This maximizes the consistency between observed and simulated data.

3. Validation and Evaluation of Convection-Permitting Simulations

The CP-RegCM4-NH evaluation is mainly focused on the autumn (SON) and summer (JJA) seasons, since convective systems and extreme events dominate during these seasons over the regions of interest. HPEs and associated flash floods are the most dangerous meteorological hazards affecting Mediterranean countries, causing extensive mortality and hundreds of millions of euros in damages every year. The Mediterranean basin and, in particular, the surrounding mountainous coastal regions are often affected by these phenomena, especially in autumn [93]. The Mediterranean Sea is a source of heat and moisture surrounded by steep orography, which favours the frequent occurrence of heavy precipitation, mainly of convective nature [94]. Under climate change, the intensity and frequency of these HPEs is expected to increase [54,60,95,96].

3.1. Evaluation of Spatial Patterns and Spatial Variability of Precipitation

Figures 6 and 7 compare the spatial distribution of daily and hourly precipitation indices (Table 2) between observations and models, for SON and JJA means over the period 2000–2009 for the 3 km and 12 km RegCM4-NH experiments, respectively. Both SON and JJA are characterised by more intense precipitation over topography. As seen in Figure 6, both CP-RegCM4-NH and RegCM4-NH capture the observed spatial patterns of mean daily precipitation, intensity, frequency, and heavy precipitation for both summer and autumn. In SON, RegCM4-NH appears to produce more rain along the coast and valleys than over topography, particularly across the Apennines. With increasing resolution, an increase in detail is seen related to the more refined representation of topography in CP-RegCM4-NH.

Some biases can be found in CP-RegCM4-NH, such as an overestimation of precipitation intensity and heavy precipitation (p99) in SON, particularly over the orographical peaks, and an underestimation of frequency and mean seasonal precipitation in JJA. Conversely, the RegCM4-NH run shows an overestimation of frequency, an underestimation of intensity (typical of coarse-resolution convection-parameterized models), and an underestimation of heavy precipitation in both seasons; CP-RegCM4-NH achieves better performance for these metrics.

These differences between the simulations are further enhanced for hourly precipitation (Figure 7). Both in SON and JJA, RegCM4-NH largely overestimates wet-hour frequency, especially over topography, while intensity and heavy precipitation (p99.9) are underestimated. This cancellation of biases leads to a relatively good performance in simulating mean daily precipitation (Figure 6). On the other hand, CP-RegCM4-NH has reduced overestimation of wet-hour frequency and reduced underestimation of hourly intensity and heavy precipitation. However, it tends to underestimate hourly precipitation intensity over southern France, overestimate heavy hourly precipitation over the west coast of Italy in SON, and miss extremes over the Alps in JJA (Figure 7).

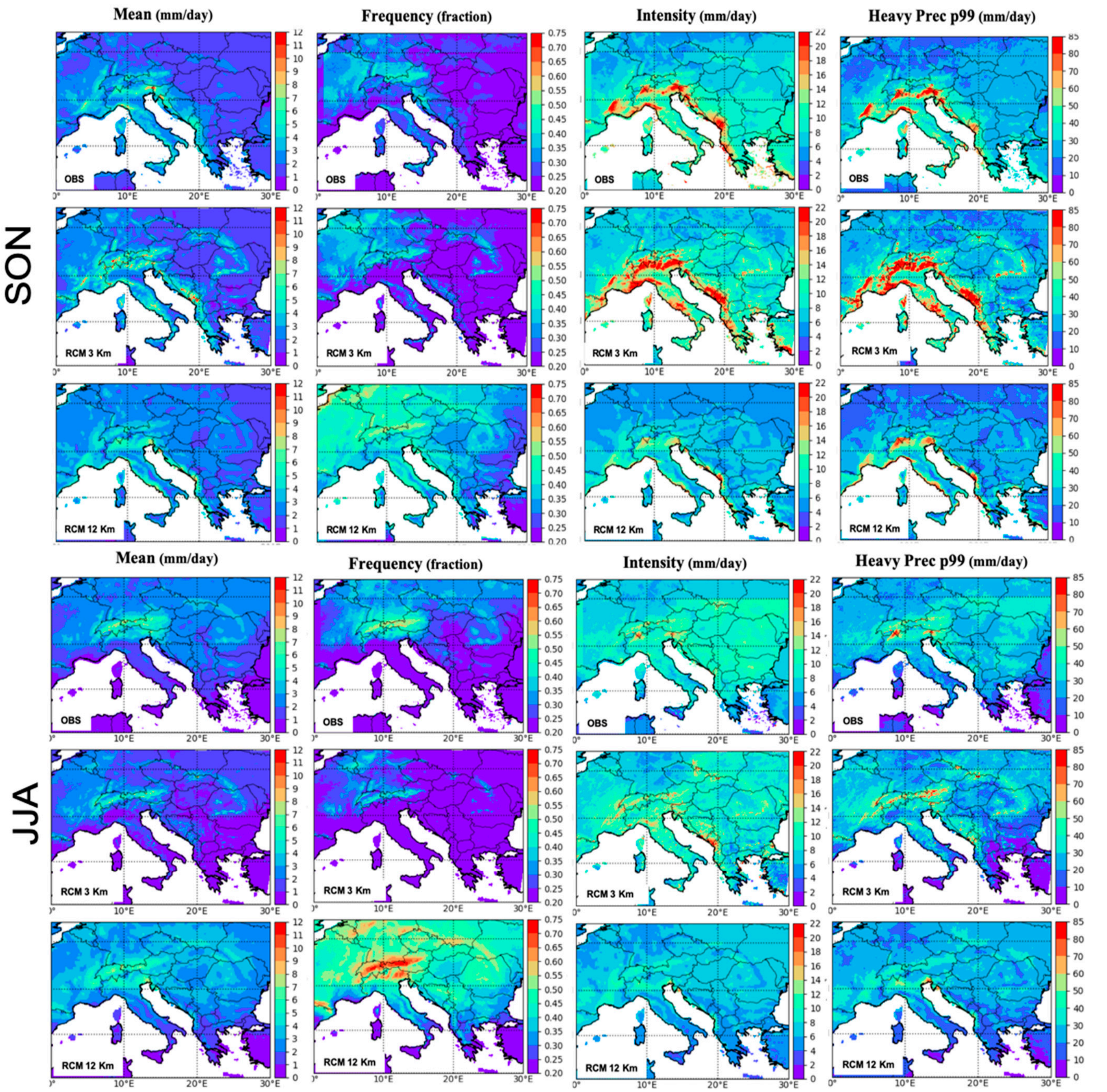

Figure 6. Seasonal mean of analysed indices (from left to right: mean precipitation, precipitation frequency, precipitation intensity, and heavy precipitation (defined as 99th percentile)) calculated for daily precipitation in the autumn (SON) and summer seasons (JJA). The results were obtained from all the observations (OBS) in Table 1 for CP-RegCM4-NH (3 km) and RegCM4-NH (12 km) model simulations.

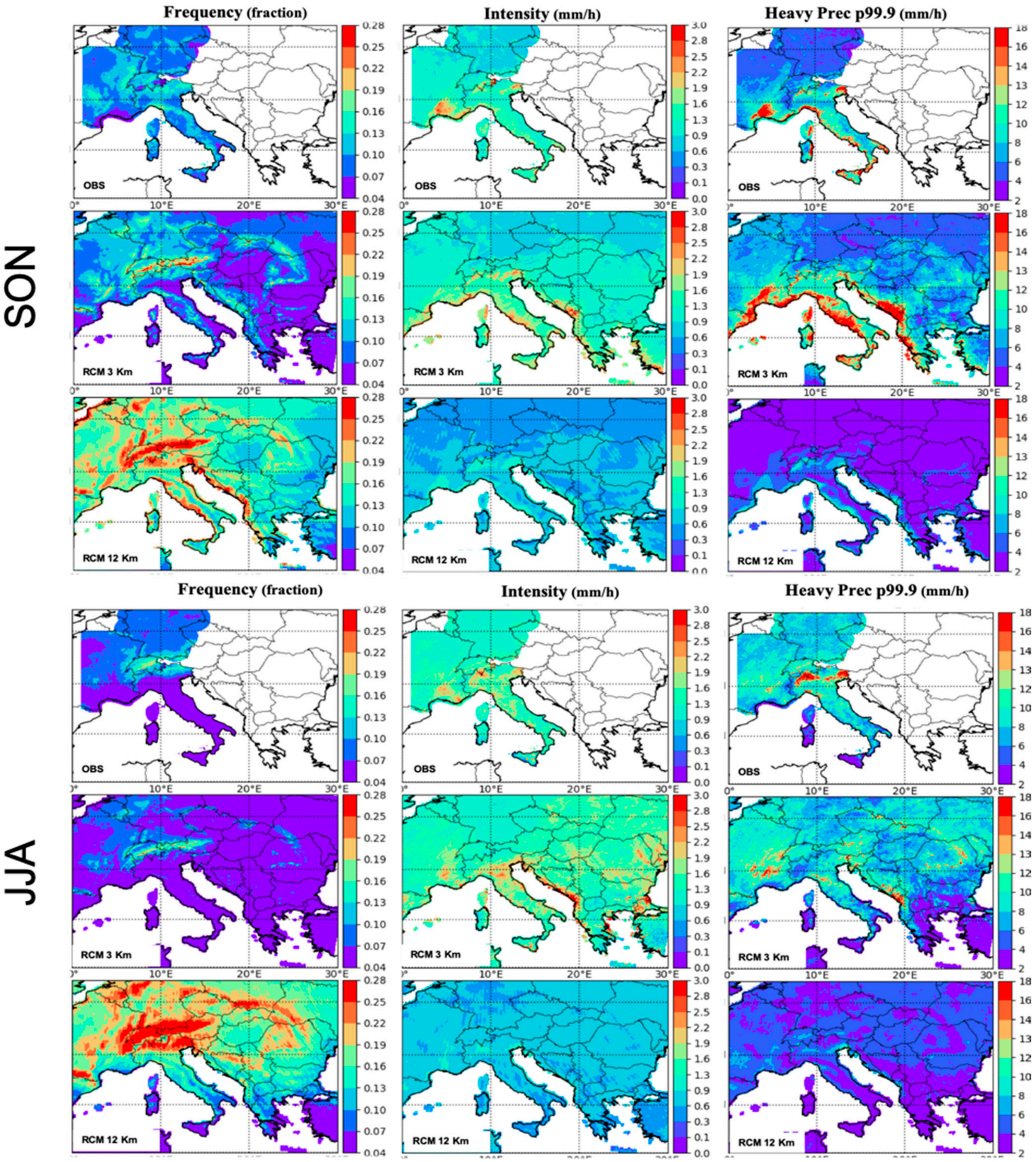

Figure 7. Similar to Figure 6, but for hourly precipitation. The observations are composed from available gridded hourly precipitation over Switzerland [74], France [8], Italy [76], and Germany [77]. Heavy hourly precipitation is defined as the 99.9th percentile of all hourly events.

The spatial representation of daily and hourly precipitation has been further assessed using Taylor diagrams [97], which combine the spatial correlation coefficient and normalized spatial variability (Table 2) for daily and hourly precipitation (Figures 8–10) over six different regions (Figure 2; Italy, France, Switzerland, Germany, the Carpathians, and Greece). For the regions where hourly observational data are available (Italy, France, Switzerland, and Germany), we only show—in addition to mean daily precipitation (Figure 8)—results at hourly scales for the other statistical indices (Figure 9), since the conclusions do not differ between daily and hourly precipitation. For the Carpathians and Greece (Figure 10), we show only daily results, due to the lack of hourly observations in these areas.

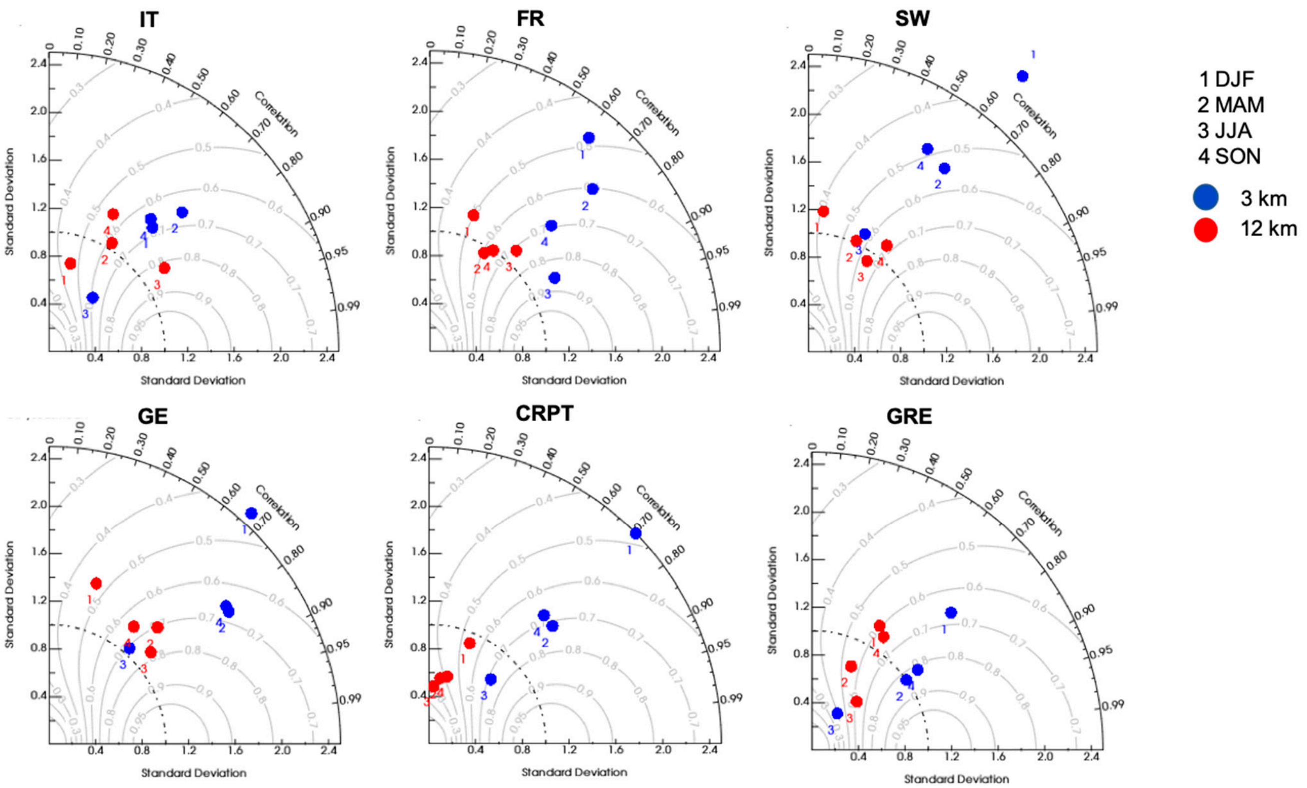

Figure 8. Spatial Taylor diagrams exploring model performance in terms of the spatial variability of mean seasonal daily precipitation over six regions—Italy (IT), France (FR), Switzerland (SW), Germany (GE), the Carpathians (CRPT), and Greece (GRE). The diagrams combine the spatial correlation (cos; azimuth angle) and the ratio of spatial variability (radius). The grey isolines show an additional measure of skill [97], with the skill score defined to vary from zero (least skilful) to one (most skilful). Red circles indicate results obtained by RegCM4-NH (12 km) simulation, while blue circles indicate results obtained by CP-RegCM4-NH (3 km) simulation.

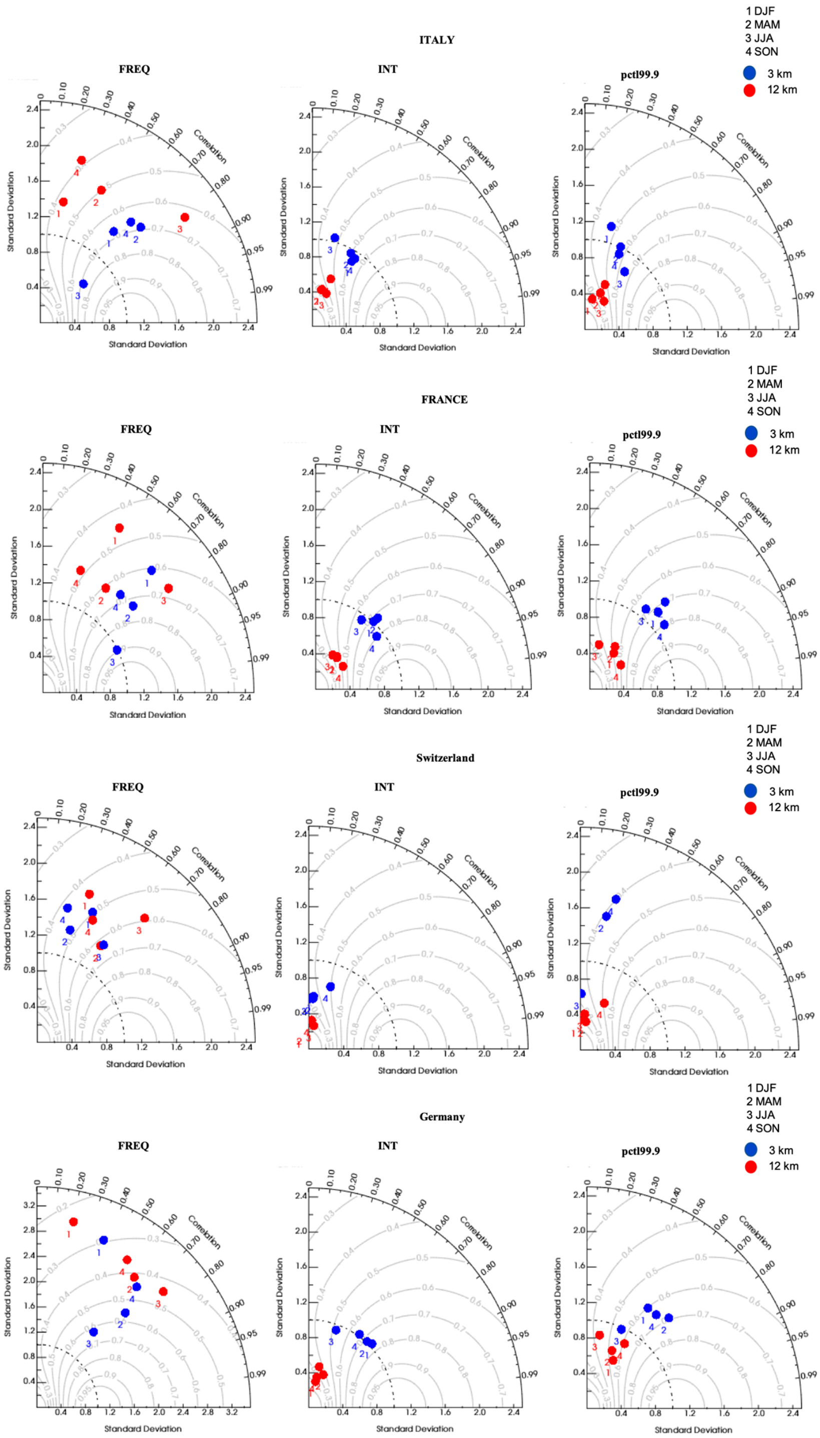

Figure 9. Spatial Taylor diagrams exploring model performance in terms of the spatial variability of seasonal hourly precipitation. The performance is explored for hourly precipitation frequency (first column), intensity (middle column), and heavy hourly precipitation (defined as 99.9th of all hourly precipitation events; last column) over four regions—Italy, France, Switzerland, and Germany (from top to bottom). The diagrams combine the spatial correlation (cos; azimuth angle), and the ratio of spatial variability (radius). The grey isolines show an additional measure of skill [97], with the skill score defined to vary from zero (least skilful) to one (most skilful). Red circles indicate results obtained by the RegCM4-NH simulation (12 km), while blue circles indicate results obtained by the CP-CP-RegCM4-NH simulation (3 km).

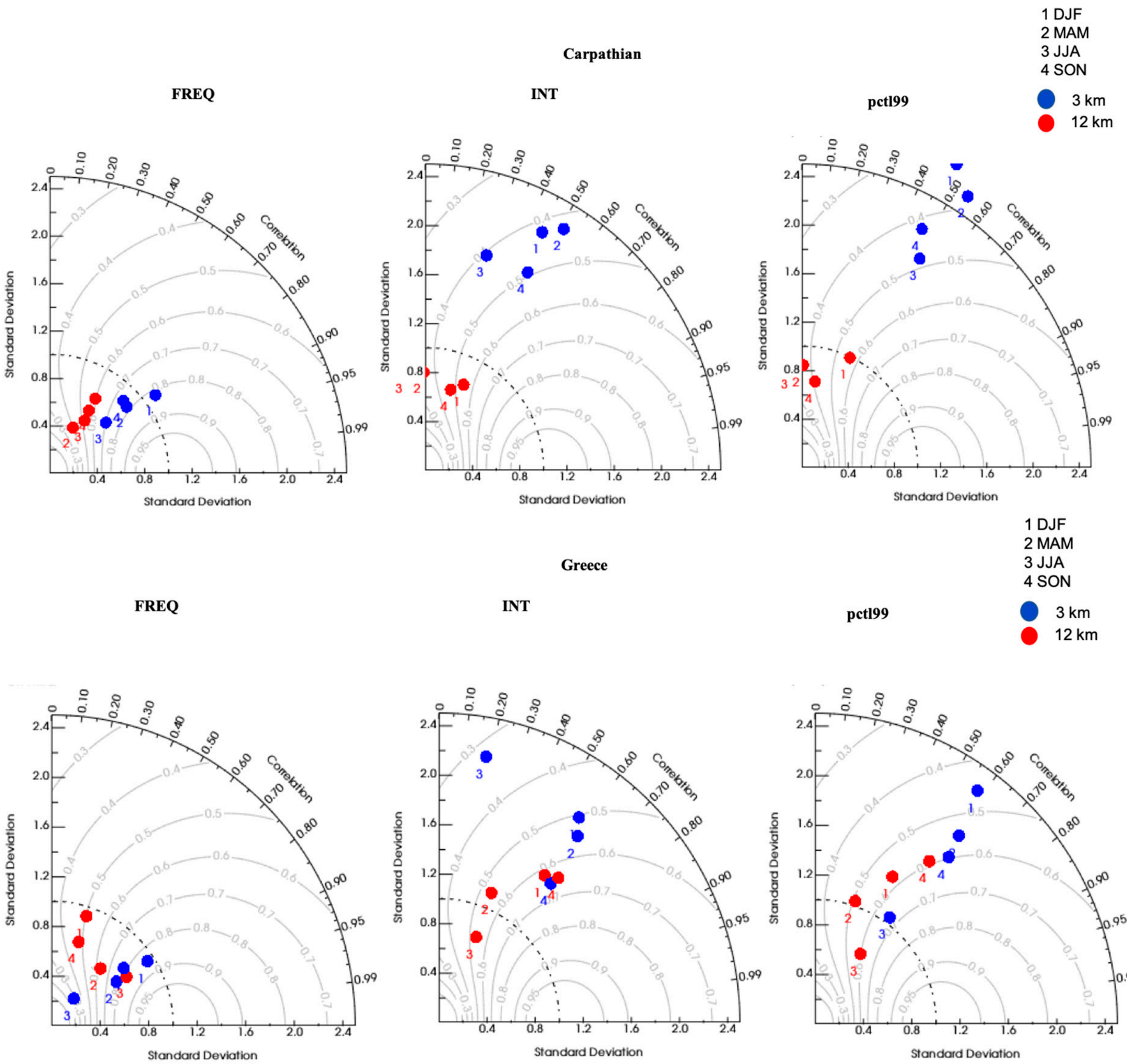

Figure 10. Similar to Figure 9, but for the Carpathians and Greece at a daily scale.

Except over Switzerland, where both simulations show a low correlation coefficient, for all the other regions and indices, CP-RegCM4-NH increases the spatial correlation compared to RegCM4-NH, with a correlation coefficient above 0.5 for most indices and seasons (Figures 8 and 9). The largest spatial correlations can be found for wet-hour intensity and hourly extremes over France, Germany, and Italy (Figure 9).

The frequency index is where the spatial correlation coefficients vary the most among seasons and regions. Over the Carpathians, the correlation coefficients are above 0.5 for wet-hour frequency, while they show lower values for the daily intensity and heavy precipitation indices (Figure 10). It is worth mentioning that the Carpathian and Greece basins are characterised by a very complex topography and, as already mentioned in paragraph 2.2, the lack of dense high-resolution observations could strongly affect the comparison between models. However, in general, the higher-resolution simulation produces higher spatial correlations for the frequency index, while for all other indices, the correlation coefficients are comparable between the two simulations.

Focusing on normalized spatial variability (Table 2), Figures 8–10 show a larger difference between the two model simulations, clearly due to their different resolutions. Figure 9 shows that RegCM4-NH underestimates the spatial variability of precipitation intensity and heavy hourly precipitation in all regions and seasons, and overestimates the observed spatial variability of wet-hour frequency. This is consistent with the substantial underestimation of precipitation intensity and overestimation of frequency in Figures 6 and 7. On the other hand, the 3 km CP-RegCM4-NH produces a spatial variability in precipitation intensity and heavy hourly precipitation more in line with the observed one, although with an overestimation over the Carpathians and Greece (Figure 10) and an underestimation over Switzerland.

As we already mentioned, part of these model errors over Switzerland can be also explained by observational uncertainties due to the sparse observational networks over higher altitudes, the interpolation methods used to produce gridded datasets, and the lack of an undercatch gauge correction. For the Carpathians and Greece, we compared the results mainly with satellite measurements, and differences found could be partially explained by the large uncertainties introduced by the different measurement techniques and algorithms used to retrieve precipitation (see Section 2.2).

Overall, we can conclude that the high-resolution CP-RegCM4-NH produces more realistic precipitation patterns and variability than the coarser-resolution RegCM4-NH, particularly when looking at hourly precipitation metrics.

3.2. Evaluation of Areal Mean and Distribution of Precipitation Uncertainties

The uncertainties in model simulations are presented in Figures 11 and 12 using box plots for both daily and hourly precipitation. The figures report the spread in relative bias across grid points for different indices (Table 2) in all seasons and for six regions (Italy, France, Switzerland, Germany, the Carpathians, and Greece), with the box plots showing the median (black line) along with the 5th, 25th, 75th, and 95th percentiles.

As reference data for both daily and hourly precipitation, we use GRIPHO for Italy; COMEPHORE for France; RdisaggH for Switzerland; RADKLIM for Germany; and the ensemble mean of the HMR, PERSIANN, CHIRPS, and CMORPH for the Carpathians and Greece.

The spread of relative bias in daily precipitation and indices are presented in Figure 11. For Italy, France, and Germany during winter, spring, and autumn, relative biases are much smaller than for Switzerland, the Carpathians and Greece. In particular, over those regions, frequency, intensity, and p99 biases are mostly in the acceptable range of observational uncertainty, particularly for CP-RegCM4-NH. In the summer season, the model exhibits higher daily precipitation biases both at high- and coarse-resolution over all regions, also showing the largest difference between the coarse and the high resolution (Figure 11).

In general, the coarse-resolution simulation tends to overestimate precipitation mean and daily frequency and underestimate daily intensity and heavy precipitation in all areas and seasons. On the other hand, the high resolution shows an overestimation of intensity and heavy precipitation, but in general, achieves a reduction of the relative bias compared to the coarse resolution model in terms of median and spatial bias range.

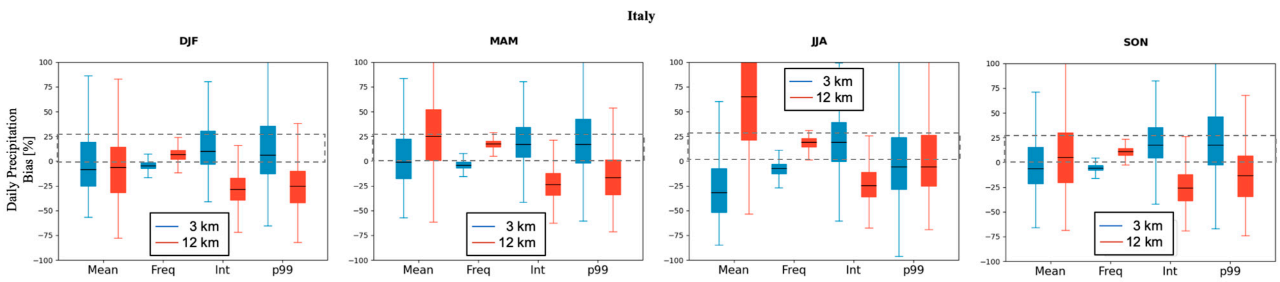

Figure 11. *Cont.*

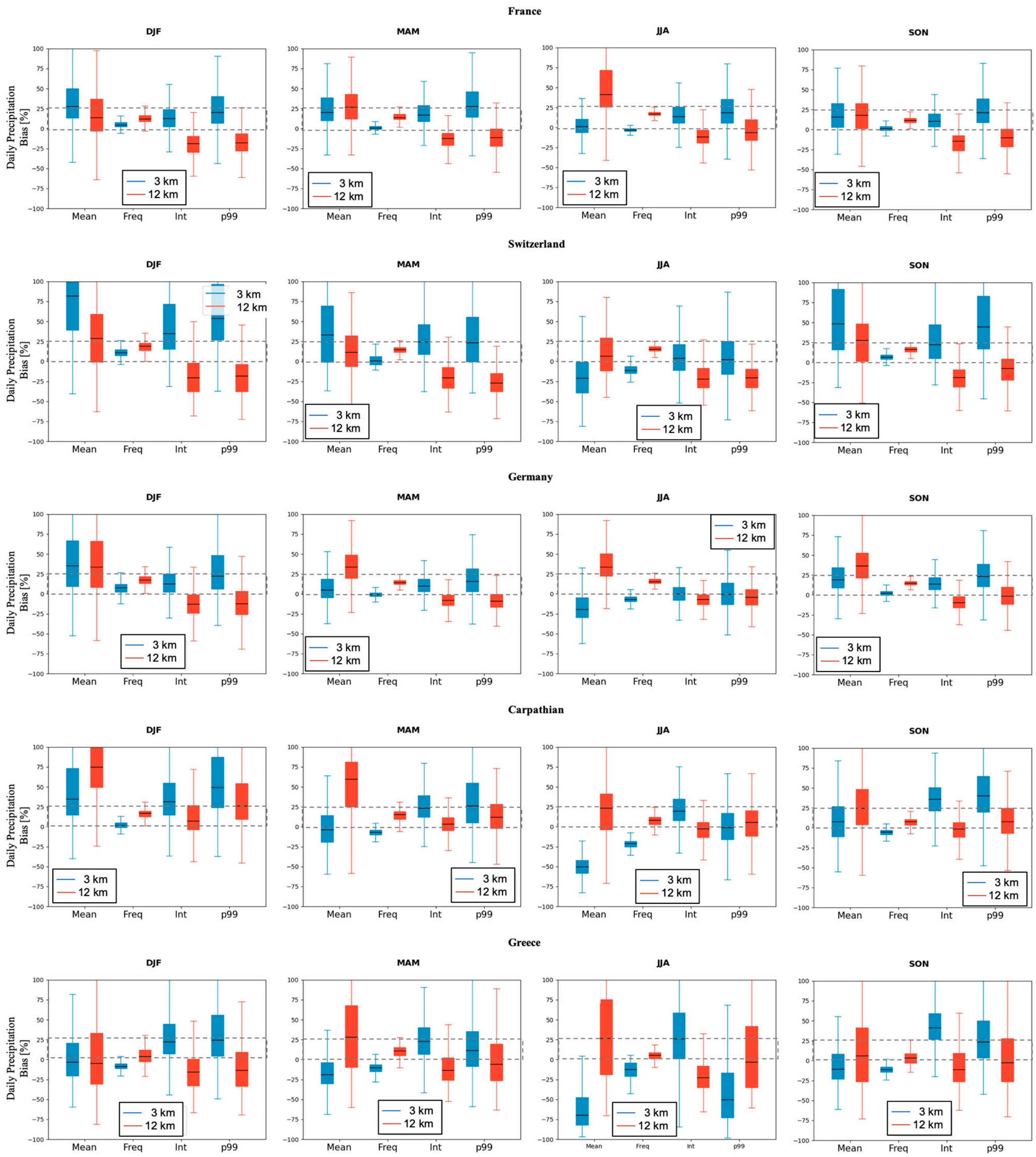

Figure 11. Box plots of 12 km (red) and 3 km (blue) model relative biases for indices presented in Table 2 for daily precipitation over six regions—Italy, France, Switzerland, Germany, the Carpathians, and Greece—for all seasons. The dashed black line indicates the acceptable uncertainty range (0–+/−25%) of observations due to the possible systematic errors discussed in Section 2.2.

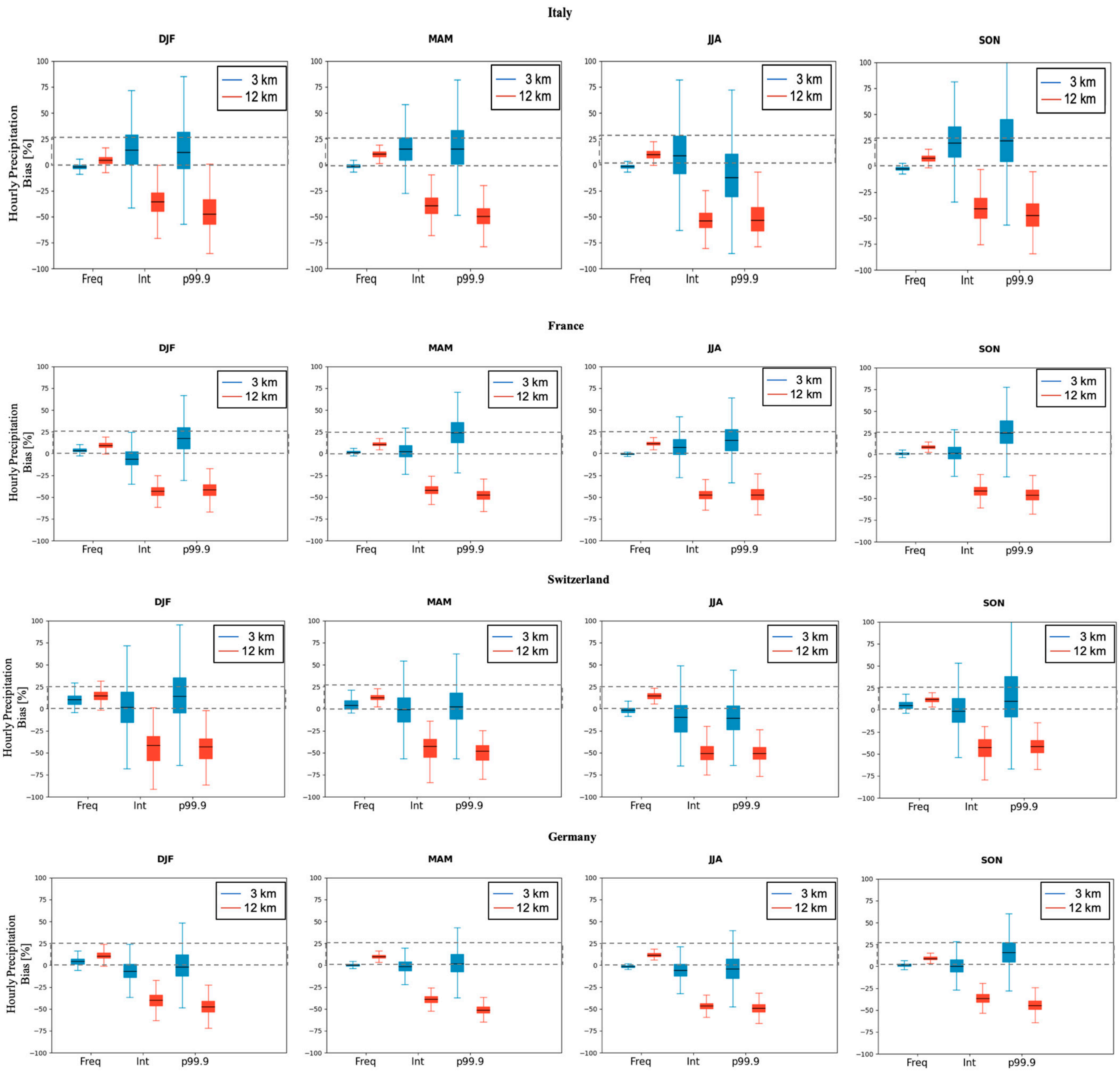

Figure 12. Similar to Figure 11, but for hourly precipitation over four regions: Italy, France, Switzerland, and Germany. Heavy hourly precipitation is defined as the 99.9th percentile (p99.9) of all events.

The spread of hourly precipitation relative biases are presented in Figure 12 for Italy, France, Switzerland, and Germany. Again, in all seasons, the coarse resolution results show an overestimation of frequency and underestimation of intensity and heavy precipitation compared to the high resolutions, with the latter performing better for wet-hour frequency and intense precipitation. The heavy precipitation is also captured quite well by CP-RegCM4-NH in all seasons except summer. In summer, over Switzerland and Italy, heavy precipitation (p99.9) also tends to be underestimated by the high-resolution simulations.

It is worth mentioning that model biases can be reduced by regionally specific tuning and model configuration, as shown by Ref. [51]. In addition, as mentioned, the observational databases used for the different regions differ from each other in many aspects and suffer from well-known issues related to station density, radar masking, and retrieving limitations (see Section 2.2). Therefore, conclusions about model errors have to take these issues into proper consideration.

3.3. PDF at Hourly and Daily Scale

Probability density functions (PDFs) of daily and hourly simulated and observed precipitation for the different regions are shown in Figures 13 and 14 respectively. The highest observed daily precipitations in the tails of the PDFs range between 200 mm (CRPT) and 600 mm (north Italy (NI) and South of France (SF)) (Figure 13, green dots), while for hourly precipitation, the range is between 100 mm (Germany) and 200 mm (Italy and France) (Figure 14).

The highest daily events in NI and SF seem to be well reproduced by the CP-RegCM4-NH simulation (blue dots), much better than RegCM4-NH 12-km (red dots). In general, for daily precipitations (Figure 13), the coarse simulation at 12 km underestimates the precipitation occurrences for the high thresholds, thereby missing the extremes. Conversely, CP-RegCM4-NH shows a tendency to overestimate the distributions' tails. The model simulations present different behaviours with respect to the other regions only over the Carpathians and Greece, but this may be affected by the fact that over these regions, the observations are based on satellite data, and therefore could present substantial uncertainties, particularly for extreme events (see Section 2.2).

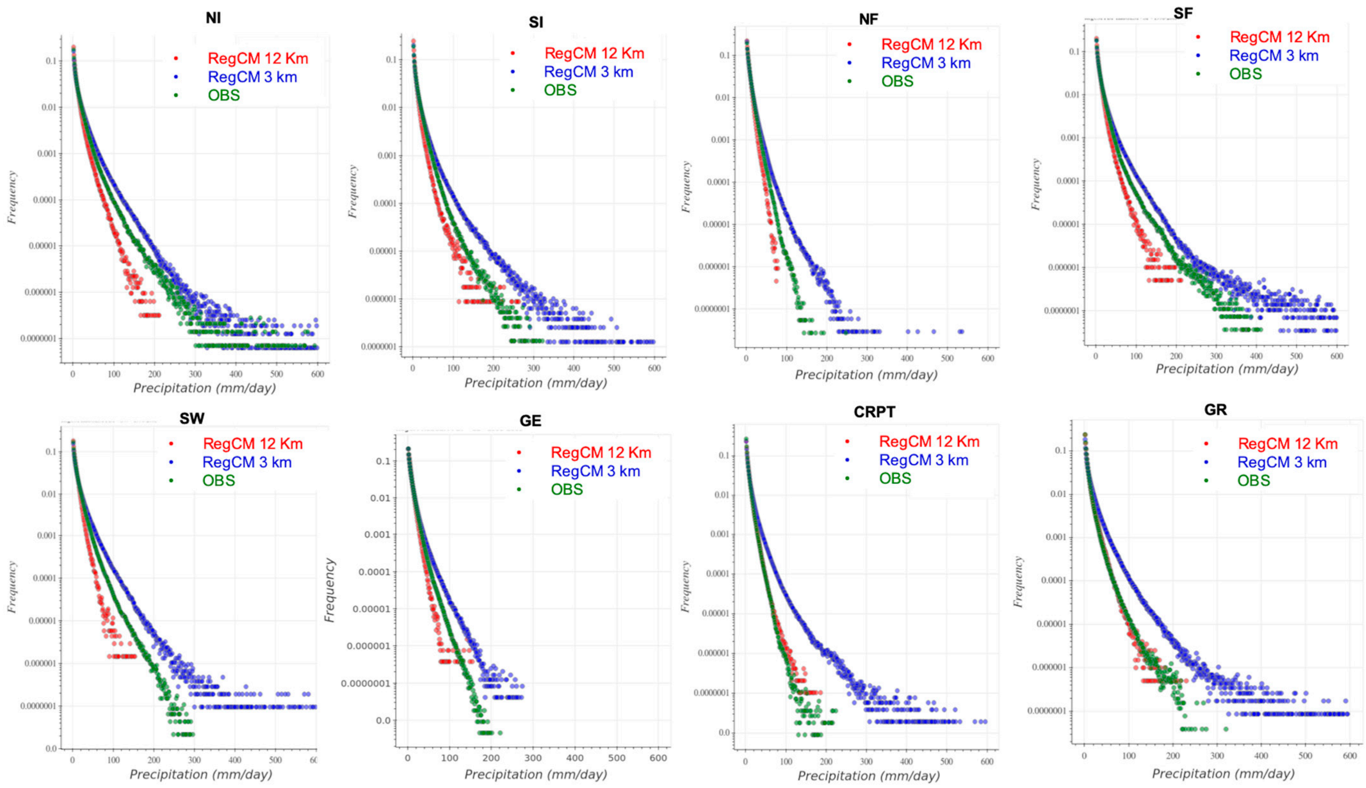

Figure 13. Probability density function (PDF) of daily precipitation over North and South Italy (NI, SI), North and South France (NF, SF), Switzerland (SW), Germany (GE), the Carpathians (CRPT), and Greece (GR). CP-RCM simulation at 3 km is in blue, RCM at 12 km is in red, and observations are in green. GRIPHO dataset has been used for Italy; COMEPHORE for France; RdisaggH for Switzerland; RADKLIM for Germany; and the ensemble mean of HMR, PERSIANN, CHIRPS, and CMORPH for the Carpathians and Greece.

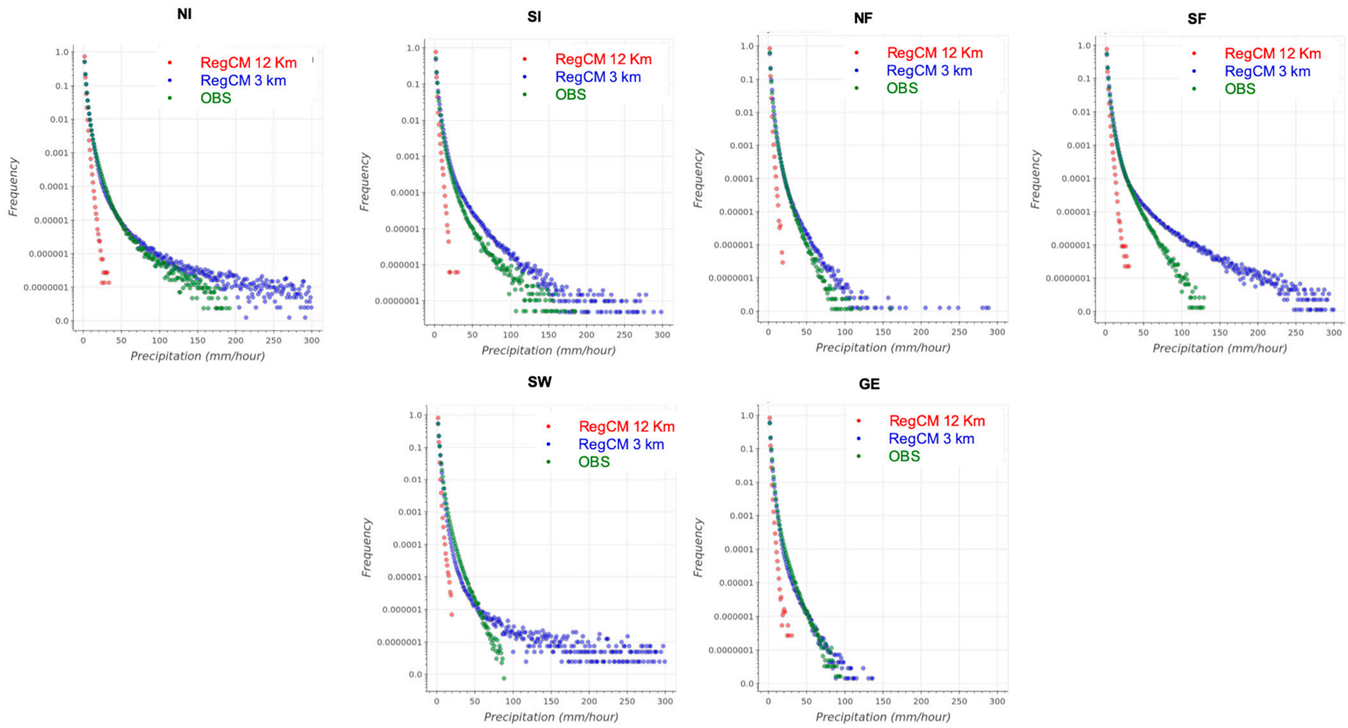

Figure 14. Similar to Figure 13, but for hourly precipitation. The observations are composed from available gridded hourly precipitation over North and South Italy (NI, SI) (GRIPHO [76]), North and South France (NF, SF) (COMEPHORE [8]), Switzerland (SW) (RADKLIM [74]), and Germany (GE) [75].

We also highlight that better results over northern Italy with respect to southern Italy are partially a consequence of the fact that the GRIPHO dataset is generated from a non-uniform station network, with a higher density of rain gauges in the northern part of the country than in the central and southern regions. Again, the hourly precipitation PDFs in Figure 14 show an underestimation compared to the observed distribution by the coarse-resolution model (red dots), which completely misses the extremes. Conversely, CP-RegCM4-NH is much closer to the observations, showing more realistic extremes, but producing longer tails than observed, particularly over Switzerland. This tendency of convection-permitting models to overestimate the intensity of extremes has been found in previous work [6,47], and may be due to the fact that convection is not entirely resolved at the few km resolution, generating excessively deep and wide updrafts and insufficient mixing [98,99]; moreover, the occurrence of sporadic numerical point storms might also affect the simulations [100,101].

4. Discussion and Conclusions

This study presents an evaluation of precipitation in the first application of RegCM4-NH [60] in climate simulations at the convection-permitting scale conducted within the CORDEX-FPS dedicated to convection and the ongoing H2020 European Climate Prediction System (EUCP) project EUCP. We have assessed simulations over three different domains in the Mediterranean area at a horizontal grid spacing of 3 km against observational datasets and an intermediate resolution driving simulation at 12 km grid spacing with the non-hydrostatic model RegCM4-NH. The main difference between the coarse- and high-resolution simulations is the treatment of convection, where this is parameterized in the former and explicitly resolved in the latter. The simulations are driven by the ERA-Interim reanalysis through a double nesting procedure and are integrated over a 10-year period (2000–2009). The model performance is assessed using several precipitation metrics: mean daily precipitation; daily/hourly precipitation intensity and frequency, and heavy daily and hourly precipitation (defined as the 99th and 99.9th percentile of all daily or hourly precipitation events, respectively).

In general, although some differences and biases are present, the observed spatial patterns and variability of precipitation over the analysis domains are represented quite well by RegCM4-NH, both at 12 km and 3 km resolution on both daily and hourly scales. The coarse-resolution model tends to overestimate the frequency, underestimate the intensity of both daily and hourly precipitation, and, in particular, underestimate the intensity of extremes. The CP-RegCM4-NH simulations considerably improve these biases, particularly at the hourly time scale. At the daily scale, results are highly region dependent. The best results can be found over Italy, France, and Germany, while the largest biases are over Switzerland, the Carpathians, and Greece, especially during the summer season (Figure 11). At the hourly scale, the improvement in the CP simulation for precipitation intensity, extreme indices, and spatial distribution is clearer than for the daily scale. Analysis of daily and hourly precipitation PDFs over different regions shows that the representation of extreme events is greatly improved in CP-RegCM4-NH, particularly at the hourly time scale. However, the tail of the distribution is somewhat more extended than in the observations; this drawback of the model needs to be addressed in future work.

As a general assessment, in the high-resolution simulations with CP-RegCM4-NH, the overall results show good performance of the model at the kilometre scale, at least in the domains analysed. Our study represents the first step towards assessing the ability of CP-RegCM-NH to simulate precipitation over different Mediterranean and European regions when run in climate mode. Our results, based on a newly developed CP-RCM and a suite of high-resolution observational datasets, are in line with previous applications of CP-RCMs [2,7,9,35,50] and confirm the improved performance of convection-permitting models with respect to coarser-resolution ones in simulating important characteristics of daily and hourly precipitation and, most importantly, extremes.

Some general considerations are necessary in the interpretation of our results. First, RegCM4-NH is a relatively new development, and this is an initial application in climate mode at a CP resolution. As such, in future simulations, there is ample space for ameliorating some of the model deficiencies evidenced in the present simulations. The availability of high-resolution, high-quality observational datasets is paramount for a robust evaluation of high-resolution models, and often, such observations are not easily available or accessible. Uncertainties in in situ data are mostly related to low station density and choice of gridding technique, which means different datasets can have significantly different climatologies, especially in areas with low data availability [82]. On the other hand, remotely based products depend on the retrieval algorithms employed to estimate precipitation characteristics.

Another key aspect to consider is that many processes that occur on sub-kilometre scales—such as microphysical processes within clouds, atmospheric turbulence, and radiative transfer processes—are still parametrized in CP models, but available parameterization schemes have frequently been developed for coarser-resolution models, and thus may still require further modifications for use at kilometre scales. A final but very important consideration is that kilometre-scale models still operate in the grey-zone of turbulent motion, which means that convection is not fully resolved, for example, with updrafts being too deep and too wide with insufficient mixing. Current research is focused on the development of scale-sensitive turbulence schemes, which should mitigate systematic biases in the planetary boundary layer and shallow and deep convective processes in kilometre-scale models [102].

Despite these issues, our results provide encouraging indications towards the use of the RegCM4-NH non-hydrostatic system for high-resolution regional climate studies, and we are continuing to develop the model with the implementation and testing of new dynamical and physical schemes and the identification of optimal model configurations over different regions.

Author Contributions: Conceptualization, P.S. and E.P.; data curation, P.S., E.P., J.A.T.A. and G.G.; formal analysis, P.S.; investigation, P.S.; methodology, P.S. and E.P.; resources, G.G.; software, G.G.; supervision, E.C. and F.G.; validation, P.S.; writing—original draft, P.S.; writing—review and editing, P.S., E.P., J.A.T.A., E.C. and F.G. All authors have read and agreed to the published version of the manuscript.

Funding: This research was founded by the European Climate Prediction system project (EUCP H2020, Grant number: 776613).

Institutional Review Board Statement: Not applicable.

Informed Consent Statement: Not applicable.

Data Availability Statement: Not applicable.

Acknowledgments: The ICTP acknowledge funding from the European Climate Prediction system project support (EUCP H2020, GA number: 776613). The authors acknowledge the WCRPCORDEX-FPS on Convective phenomena at high resolution over Europe and the Mediterranean (FPSCONV). The authors gratefully acknowledge the Consorzio Interuniversitario per il Calcolo Automatico dell'Italia Nord Orientale (CINECA) super-computing centre (Bologna, Italy) for computing resources, and the CETEMPS, University of L'Aquila, for allowing access to the Italian database of precipitation which GRIPHO is based on. The authors acknowledge the following institutes for providing observations: MeteoSwiss; Meteo France; DWD Germany; the Climate Hazards Group (https://www.chc.ucsb.edu/data, accessed on 26 March 2021); the Center for Hydrometeorology and Remote Sensing (CHRS) at the University of California, Irvine (UCI); and the NOAA (https://www.cpc.ncep.noaa.gov/products/janowiak/cmorph_description.html, accessed on 16 December 2020). The authors acknowledge the usage of the CHIRPS data set from the Climate Hazards Group (https://www.chc.ucsb.edu/data, accessed on 26 March 2021); PERSIANN-Cloud Classification System (PERSIANN-CCS) by the Center for Hydrometeorology and Remote Sensing (CHRS) at the University of California, Irvine (UCI); and CMORPH (CPC MORPHing technique) by NOAA (https://www.cpc.ncep.noaa.gov/products/janowiak/cmorph_description.html, accessed on 3 May 2021).

Conflicts of Interest: The authors declare no conflict of interest.

References

1. Weisman, M.L.; Skamarock, W.C.; Klemp, J.B. The resolution dependence of explicitly modeled convective systems. *Mon. Weather Rev.* **1997**, *125*, 527–548. [CrossRef]
2. Ban, N.; Schmidli, J.; Schär, C. Evaluation of the convection-resolving regional climate modeling approach in decade-long simulations. *J. Geophys. Res. Atmos.* **2014**, *119*, 7889–7907. [CrossRef]
3. Kendon, E.J.; Roberts, N.M.; Senior, C.A.; Roberts, M.J. Realism of rainfall in a very high-resolution regional climate model. *J. Clim.* **2012**, *25*, 5791–5806. [CrossRef]
4. Kendon, E.J.; Roberts, N.M.; Fowler, H.; Roberts, M.J.; Chan, S.C.; Senior, C.A. Heavier summer downpours with climate change revealed by weather forecast resolution model. *Nat. Clim. Chang.* **2014**, *4*, 570–576. [CrossRef]
5. Leutwyler, D.; Lüthi, D.; Ban, N.; Fuhrer, O.; Schär, C. Evaluation of the convection-resolving climate modeling approach on continental scales. *J. Geophys. Res. Atmos.* **2017**, *122*, 5237–5258. [CrossRef]
6. Prein, A.F.; Rasmussen, R.M.; Ikeda, K.; Liu, C.; Clark, M.P.; Holland, G.J. The future intensification of hourly precipitation extremes. *Nat. Clim. Chang.* **2017**, *7*, 48–52. [CrossRef]
7. Berthou, S.; Kendon, E.J.; Chan, S.C.; Ban, N.; Leutwyler, D.; Schär, C.; Fosser, G. Pan-European climate at convection-permitting scale: A model intercomparison study. *Clim. Dyn.* **2018**, *55*, 35–59. [CrossRef]
8. Fumière, Q.; Déqué, M.; Nuissier, O.; Somot, S.; Alias, A.; Caillaud, C.; Laurantin, O.; Seity, Y. Extreme rainfall in Mediterranean France during the fall: Added value of the CNRM-AROME Convection-Permitting Regional Climate Model. *Clim. Dyn.* **2020**, *55*, 77–91. [CrossRef]
9. Prein, A.F.; Langhans, W.; Fosser, G.; Ferrone, A.; Ban, N.; Goergen, K.; Keller, M.; Tölle, M.; Gutjahr, O.; Feser, F.; et al. A review on regional convection-permitting climate modeling: Demonstrations, prospects and challenges. *Rev. Geophys.* **2015**, *53*, 323–361. [CrossRef]
10. Pedersen, C.A.; Winther, J.-G. Intercomparison and validation of snow albedo parameterization schemes in climate models. *Clim. Dyn.* **2005**, *25*, 351–362. [CrossRef]
11. Déqué, M.; Rowell, D.P.; Luethi, D.; Giorgi, F.; Christensen, J.H.; Rockel, B.; Jacob, D.; Kjellstroem, E.; De Castro, M.; Hurk, B.V.D. An intercomparison of regional climate simulations for Europe: Assessing uncertainties in model projections. *Clim. Chang.* **2007**, *81*, 53–70. [CrossRef]

12. Brockhaus, P.; Lüthi, D.; Schär, C. Aspects of the diurnal cycle in a regional climate model. *Meteorol. Z.* **2008**, *17*, 433–443. [CrossRef]
13. Hohenegger, C.; Brockhaus, P.; Schär, C. Towards climate simulations at cloud-resolving scales. *Meteorol. Z.* **2008**, *17*, 383–394. [CrossRef]
14. Hanel, M.; Buishand, T.A. On the value of hourly precipitation extremes in regional climate model simulations. *J. Hydrol.* **2010**, *393*, 265–273. [CrossRef]
15. Dirmeyer, P.A.; Cash, B.A.; Kinter, J.L., III; Jung, T.; Marx, L.; Satoh, M.; Stan, C.; Tomita, H.; Towers, P.; Wedi, N.; et al. Simulating the diurnal cycle of rainfall in global climate models: Resolution versus parameterization. *Clim. Dyn.* **2012**, *39*, 399–418. [CrossRef]
16. Déqué, M.; Somot, S. Analysis of heavy precipitation for France using high resolution ALADIN RCM simulations. *Időjárás* **2008**, *112*, 179–190.
17. Torma, C.; Giorgi, F.; Coppola, E. Added value of regional climate modeling over areas characterized by complex terrainprecipitation over the Alps. *J. Geophys. Res. Atmos.* **2015**, *120*, 3957–3972. [CrossRef]
18. Ruti, P.M.; Somot, S.; Giorgi, F.; Dubois, C.; Flaounas, E.; Obermann, A.; Dell'Aquila, A.; Pisacane, G.; Harzallah, A.; Lombardi, E.; et al. MED-CORDEX initiative for Mediterranean climate studies. *Bull. Am. Meteorol. Soc.* **2016**, *97*, 1187–1208. [CrossRef]
19. Prein, A.F.; Gobiet, A.; Truhetz, H.; Keuler, K.; Goergen, K.; Teichmann, C.; Maule, C.F.; Van Meijgaard, E.; Déqué, M.; Nikulin, G.; et al. Precipitation in the EURO-CORDEX 0.11° and 0.44° simulations: High resolution, high benefits? *Clim. Dyn.* **2016**, *46*, 383–412. [CrossRef]
20. Fantini, A.; Raffaele, F.; Torma, C.; Bacer, S.; Coppola, E.; Giorgi, F.; Ahrens, B.; Dubois, C.; Sanchez, E.; Verdecchia, M. Assessment of multiple daily precipitation statistics in ERA-Interim driven Med-CORDEX and EURO-CORDEX experiments against high resolution observations. *Clim. Dyn.* **2018**, *51*, 877–900. [CrossRef]
21. Grell, G.A.; Schade, L.; Knoche, R.; Pfeiffer, A.; Egger, J. Nonhydrostatic climate simulations of precipitation over complex terrain. *J. Geophys. Res. Earth Surf.* **2000**, *105*, 29595–29608. [CrossRef]
22. Ducrocq, V.; Ricard, D.; Lafore, J.P.; Orain, F. Storm-scale numerical rainfall prediction for five precipitating events over France: On the importance of the initial humidity field. *Weather Forecast.* **2002**, *17*, 1236–1256. [CrossRef]
23. Richard, E.; Buzzi, A.; Zaengl, G. Quantitative precipitation fore- casting in the Alps: The advances achieved by the mesoscale alpine programme. *Q. J. R. Meteorol. Soc.* **2007**, *133*, 831–846. [CrossRef]
24. Done, J.; Davis, C.A.; Weisman, M. The next generation of NWP: Explicit forecasts of convection using the weather research and forecasting (WRF) model. *Atmos. Sci. Lett.* **2004**, *5*, 110–117. [CrossRef]
25. Lean, H.W.; Clark, P.; Dixon, M.; Roberts, N.M.; Fitch, A.; Forbes, R.; Halliwell, C. Characteristics of High-Resolution Versions of the Met Office Unified Model for Forecasting Convection over the United Kingdom. *Mon. Weather Rev.* **2008**, *136*, 3408–3424. [CrossRef]
26. Nuissier, O.; Ducrocq, V.; Ricard, D.; Lebeaupin, C.; Anquetin, S. A numerical study of three catastrophic precipitating events over southern France. I: Numerical framework and synoptic ingredients. *Q. J. R. Meteorol. Soc.* **2008**, *134*, 111–130. [CrossRef]
27. Weisman, M.L.; Davis, C.; Wang, W.; Manning, K.W.; Klemp, J.B. Experiences with 0–36-h Explicit Convective Forecasts with the WRF-ARW Model. *Weather Forecast.* **2008**, *23*, 407–437. [CrossRef]
28. Weusthoff, T.; Ament, F.; Arpagaus, M.; Rotach, M.W. Assessing the Benefits of Convection-Permitting Models by Neighborhood Verification: Examples from MAP D-PHASE. *Mon. Weather Rev.* **2010**, *138*, 3418–3433. [CrossRef]
29. Schwartz, C.S. Reproducing the September 2013 Record-Breaking Rainfall over the Colorado Front Range with High-Resolution WRF Forecasts. *Weather Forecast.* **2014**, *29*, 393–402. [CrossRef]
30. Clark, P.; Roberts, N.; Lean, H.; Ballard, S.P.; Charlton-Perez, C. Convection-permitting models: A step-change in rainfall forecasting. *Meteorol. Appl.* **2016**, *23*, 165–181. [CrossRef]
31. Khodayar, S.; Fosser, G.; Berthou, S.; Davolio, S.; Drobinski, P.; Ducrocq, V.; Ferretti, R.; Nuret, M.; Pichelli, E.; Richard, E.; et al. A seamless weather–climate multi-model intercomparison on the representation of a high impact weather event in the western Mediterranean: HyMeX IOP12. *Q. J. R. Meteorol. Soc.* **2016**, *142*, 433–452. [CrossRef]
32. Chan, S.C.; Kendon, E.J.; Fowler, H.; Blenkinsop, S.; Roberts, N.M.; Ferro, C.A.T. The Value of High-Resolution Met Office Regional Climate Models in the Simulation of Multihourly Precipitation Extremes. *J. Clim.* **2014**, *27*, 6155–6174. [CrossRef]
33. Chan, S.C.; Kahana, R.; Kendon, E.J.; Fowler, H.J. Projected changes in extreme precipitation over Scotland and Northern England using a high-resolution regional climate model. *Clim. Dyn.* **2018**, *51*, 3559–3577. [CrossRef]
34. Fosser, G.; Khodayar, S.; Berg, P. Benefit of convection permitting climate model simulations in the representation of convective precipitation. *Clim. Dyn.* **2015**, *44*, 45–60. [CrossRef]
35. Knist, S.; Goergen, K.; Simmer, C. Evaluation and projected changes of precipitation statistics in convection-permitting WRF climate simulations over Central Europe. *Clim. Dyn.* **2018**, *55*, 325–341. [CrossRef]
36. Caillaud, C.; Somot, S.; Alias, A.; Bernard-Bouissières, I.; Fumière, Q.; Laurantin, O.; Seity, Y.; Ducrocq, V. Modelling Mediterranean heavy precipitation events at climate scale: An object-oriented evaluation of the CNRM-AROME convection-permitting regional climate model. *Clim. Dyn.* **2021**, *56*, 1717–1752. [CrossRef]
37. Shahi, N.K.; Polcher, J.; Bastin, S.; Pennel, R.; Fita, L. Assessment of the spatio-temporal variability of the added value on precipitation of convection-permitting simulation over the Iberian Peninsula using the RegIPSL regional earth system model. *Clim. Dyn.* **2022**, 1–28. [CrossRef]

38. Prein, A.F.; Gobiet, A.; Suklitsch, M.; Truhetz, H.; Awan, N.K.; Keuler, K.; Georgievski, G. Added value of vonvection permitting seasonal simulations. *Clim. Dyn.* **2013**, *41*, 2655–2677. [CrossRef]
39. Ban, N.; Schmidli, J.; Schär, C. Heavy precipitation in a changing climate: Does short-term summer precipitation increase faster? *Geophys. Res. Lett.* **2015**, *42*, 1165–1172. [CrossRef]
40. Lind, P.; Lindstedt, D.; Kjellström, E.; Jones, C. Spatial and Temporal Characteristics of Summer Precipitation over Central Europe in a Suite of High-Resolution Climate Models. *J. Clim.* **2016**, *29*, 3501–3518. [CrossRef]
41. Adinolfi, M.; Raffa, M.; Reder, A.; Mercogliano, P. Evaluation and Expected Changes of Summer Precipitation at Convection Permitting Scale with COSMO-CLM over Alpine Space. *Atmosphere* **2021**, *12*, 54. [CrossRef]
42. Lind, P.; Belušić, D.; Christensen, O.B.; Dobler, A.; Kjellström, E.; Landgren, O.; Lindstedt, D.; Matte, D.; Pedersen, R.A.; Toivonen, E.; et al. Benefits and added value of convection-permitting climate modeling over Fenno-Scandinavia. *Clim. Dyn.* **2020**, *55*, 1893–1912. [CrossRef]
43. Brisson, E.; van Weverberg, K.; Demuzere, M.; Devis, A.; Saeed, S.; Stengel, M.; van Lipzig, N.P.M. How well can a convection-permitting climate model reproduce decadal statistics of precipitation, temperature and cloud characteristics? *Clim. Dyn.* **2016**, *47*, 3043–3061. [CrossRef]
44. Chan, S.C.; Kendon, E.J.; Berthou, S.; Fosser, G.; Lewis, E.; Fowler, H.J. Europe-wide precipitation projections at convection permitting scale with the Unified Model. *Clim. Dyn.* **2020**, *55*, 409–428. [CrossRef] [PubMed]
45. Kendon, E.J.; Stratton, R.A.; Tucker, S.; Marsham, J.H.; Berthou, S.; Rowell, D.P.; Senior, C.A. Enhanced future changes in wet and dry extremes over Africa at convection-permitting scale. *Nat. Commun.* **2019**, *10*, 1794. [CrossRef]
46. Senior, C.A.; Marsham, J.H.; Berthou, S.; Burgin, L.E.; Folwell, S.S.; Kendon, E.J.; Klein, C.M.; Jones, R.G.; Mittal, N.; Rowell, D.P.; et al. Convection-Permitting Regional Climate Change Simulations for Understanding Future Climate and Informing Decision-Making in Africa. *Bull. Am. Meteorol. Soc.* **2021**, *102*, E1206–E1223. [CrossRef]
47. Kendon, E.J.; Ban, N.; Roberts, N.M.; Fowler, H.J.; Roberts, M.J.; Chan, S.C.; Evans, J.P.; Fosser, G.; Wilkinson, J.M. Do convection-permitting regional climate models improve projections of future precipitation change? *Bull. Am. Meteorol. Soc.* **2017**, *98*, 79–93. [CrossRef]
48. Lenderink, G.; Belušic, D.; Fowler, H.J.; Kjellström, E.; Lind, P.; van Meijgaard, E.; van Ulft, B.; de Vries, H. Systematic thermodynamic responses of hourly precipitation extremes in a warming experiment with a convection-permitting climate model. *Environ. Res. Lett.* **2019**, *14*, 074012. [CrossRef]
49. Fowler, H.J.; Lenderink, G.; Prein, A.F.; Westra, S.; Allan, R.P.; Ban, N.; Barbero, R.; Berg, P.; Blenkinsop, S.; Do, H.X.; et al. Anthropogenic intensification of short-duration rainfall extremes. *Nat. Rev. Earth Environ.* **2021**, *2*, 107–122. [CrossRef]
50. Ban, N.; Caillaud, C.; Coppola, E.; Pichelli, E.; Sobolowski, S.; Adinolfi, M.; Ahrens, B.; Alias, A.; Anders, I.; Bastin, S.; et al. The first multi-model ensemble of regional climate simulations at kilometer-scale resolution, part I: Evaluation of precipitation. *Clim. Dyn.* **2021**, *57*, 275–302. [CrossRef]
51. Coppola, E.; Sobolowski, S.; Pichelli, E.; Raffaele, F.; Ahrens, B.; Anders, I.; Ban, N.; Bastin, S.; Belda, M.; Belusic, D.; et al. A first-of-its-kind multi-model convection permitting ensemble for investigating convective phenomena over Europe and the Mediterranean. *Clim. Dyn.* **2020**, *55*, 3–34. [CrossRef]
52. Hewitt, C.D.; Lowe, J.A. Toward a European Climate Prediction System. *Bull. Am. Meteorol. Soc.* **2018**, *99*, 1997–2001. [CrossRef]
53. Kendon, E.J.; Roberts, N.M.; Fosser, G.; Martin, G.M.; Lock, A.P.; Murphy, J.M.; Senior, C.A.; Tucker, S.O. Greater Future U.K. Winter Precipitation Increase in New Convection-Permitting Scenarios. *J. Clim.* **2020**, *33*, 7303–7318. [CrossRef]
54. Pichelli, E.; Coppola, E.; Sobolowski, S.; Ban, N.; Giorgi, F.; Stocchi, P.; Alias, A.; Belušić, D.; Berthou, S.; Caillaud, C.; et al. The first multi-model ensemble of regional climate simulations at kilometer-scale resolution part 2: Historical and future simulations of precipitation. *Clim. Dyn.* **2021**, *56*, 3581–3602. [CrossRef]
55. Fosser, G.; Kendon, E.J.; Chan, S.C.; Lock, A.; Roberts, N. Optimal configuration and resolution for the first convection permitting ensemble of climate projections over the UK. *Int. J. Climatol.* **2020**, *40*, 3585–3606. [CrossRef]
56. Fosser, G.; Kendon, E.J.; Stephenson, D.; Tucker, S. Convection-permitting models offer the promise of more certain extreme rainfall projections. *Geophys. Res. Lett.* **2020**, *47*, e2020GL088151. [CrossRef]
57. Manning, C.; Kendon, E.J.; Fowler, H.J.; Roberts, N.M.; Berthou, S.; Suri, D.; Roberts, M.J. Extreme windstorms and sting jets in convection-permitting climate simulations over Europe. *Clim. Dyn.* **2021**, *58*, 2387–2404. [CrossRef]
58. Dale, M.; Hosking, A.; Gill, E.; Kendon, E.; Fowler, H.; Blenkinsop, S.; Chan, S. Understanding how changing rainfall may impact on urban drainage systems; lessons from projects in the UK and USA. *Water Prac. Technol.* **2018**, *13*, 654–661. [CrossRef]
59. Giorgi, F.; Coppola, E.; Solmon, F.; Mariotti, L.; Sylla, M.B.; Bi, X.; Elguindi, N.; Diro, G.T.; Nair, V.; Giuliani, G.; et al. RegCM4: Model description and preliminary tests over multiple CORDEX domains. *Clim. Res.* **2012**, *52*, 7–29. [CrossRef]
60. Coppola, E.; Stocchi, P.; Pichelli, E.; Alavez, J.A.T.; Glazer, R.; Giuliani, G.; Di Sante, F.; Nogherotto, R.; Giorgi, F. Non-Hydrostatic RegCM4 (RegCM4-NH): Model description and case studies over multiple domains. *Geosci. Model Dev.* **2021**, *14*, 7705–7723. [CrossRef]
61. Dee, D.P.; Uppala, S.M.; Simmons, A.J.; Berrisford, P.; Poli, P.; Kobayashi, S.; Andrae, U.; Balmaseda, M.A.; Balsamo, G.; Bauer, P.; et al. The ERA-Interim reanalysis: Configuration and performance of the data assimilation system. *Q. J. R. Meteorol. Soc.* **2011**, *137*, 553–597. [CrossRef]

62. Coppola, E.; Nogherotto, R.; Ciarlo', J.M.; Giorgi, F.; van Meijgaard, E.; Kadygrov, N.; Iles, C.; Corre, L.; Sandstad, M.; Somot, S.; et al. Assessment of the European Climate Projections as Simulated by the Large EURO-CORDEX Regional and Global Climate Model Ensemble. *J. Geophys. Res. Atmos.* **2021**, *126*. [CrossRef]
63. Bretherton, C.S.; McCaa, J.R.; Grenier, H. A new parameterization for shallow cumulus convection and its application to marine subtropical cloud-topped boundary layers. I. Description and 1D results. *Mon. Weather Rev.* **2004**, *132*, 864–882. [CrossRef]
64. Tiedtke, M. A comprehensive mass flux scheme for cumulus parameterization in large-scale models. *Mon. Weather Rev.* **1989**, *117*, 1779–1800. [CrossRef]
65. Tiedtke, M. Representation of Clouds in Large-Scale Models. *Mon. Weather Rev.* **1993**, *121*, 3040–3061. [CrossRef]
66. Tiedtke, M. An Extension of Cloud-Radiation Parameterization in the ECMWF Model: The Representation of Subgrid-Scale Variations of Optical Depth. *Mon. Weather Rev.* **1996**, *124*, 745–750. [CrossRef]
67. Pal, J.S.; Small, E.; Eltahir, E.A.B. Simulation of regional-scale water and energy budgets: Representation of subgrid cloud and precipitation processes within RegCM. *J. Geophys. Res. Earth Surf.* **2000**, *105*, 29579–29594. [CrossRef]
68. Kiehl, J.; Hack, J.; Bonan, G.; Boville, B.; Briegleb, B.; Williamson, D.; Rasch, P. Description of the NCAR Community Climate Model (CCM3). *NCAR Tech. Note* **1996**, *152*. [CrossRef]
69. Oleson, K.W.; Lawrence, D.M.; Bonan, G.B.; Drewniak, B.; Huang, M.; Koven, C.D.; Levis, S.; Li, F.; Riley, W.J.; Subin, Z.M.; et al. *Technical Description of Version 4.5 of the Community Land Model (CLM)*; NCAR Technical Report NCAR/TN-503+STR; National Center for Atmospheric Research: Boulder, CO, USA, 2013; p. 422. [CrossRef]
70. Zeng, X.; Zhao, M.; Dickinson, R.E. Intercomparison of bulk aerodynamic algorithms for the computation of sea surface fluxes using TOGA COARE and TAO data. *J. Clim.* **1998**, *11*, 2628–2644. [CrossRef]
71. Holtslag, A.; de Bruijn, E.; Pan, H.L. A high resolution air mass transformation model for short-range weather forecasting. *Mon. Weather Rev.* **1990**, *118*, 1561–1575. [CrossRef]
72. Hong, S.-Y.; Dudhia, J.; Chen, S.-H. A Revised Approach to Ice Microphysical Processes for the Bulk Parameterization of Clouds and Precipitation. *Mon. Weather Rev.* **2004**, *132*, 103–120. [CrossRef]
73. Isotta, F.A.; Frei, C.; Weilguni, V.; Tadić, M.P.; Lassègues, P.; Rudolf, B.; Pavan, V.; Cacciamani, C.; Antolini, G.; Ratto, S.M.; et al. The climate of daily precipitation in the Alps: Development and analysis of a high-resolution grid dataset from pan-Alpine rain-gauge data. *Int. J. Clim.* **2013**, *34*, 1657–1675. [CrossRef]
74. Wüest, M.; Frei, C.; Altenhoff, A.; Hagen, M.; Litschi, M.; Schär, C. A gridded hourly precipitation dataset for Switzerland using rain-gauge analysis and radar-based disaggregation. *Int. J. Clim.* **2009**, *30*, 1764–1775. [CrossRef]
75. Tabary, P.; Dupuy, P.; Lhenaff, G.; Gueguen, C.; Moulin, L.; Laurantin, O.; Merlier, C.; Soubeyroux, J.M. A 10-year (1997–2006) reanalysis of quantitative precipitation estimation over France: Methodology and first results. *IAHS-AISH Publ.* **2012**, *351*, 255–260.
76. Fantini, A. Climate Change Impact on Flood Hazard over Italy. Ph.D. Thesis, University of Trieste, Trieste, Italy, 2019. Available online: http://hdl.handle.net/11368/2940009 (accessed on 24 May 2020).
77. Winterrath, T.; Brendel, C.; Hafer, M.; Junghänel, T.; Klameth, A.; Walawender, E.; Weigl, E.; Becker, A. *Erstellung einer Radargestützten Niederschlagsklimatologie*; German Weather Service Reports; Deutschen Wetterdienstes: Offenbach, Germany, 2017.
78. Landelius, T.; Dahlgren, P.; Gollvik, S.; Jansson, A.; Olsson, E. A high-resolution regional reanalysis for Europe. Part 2: 2D analysis of surface temperature, precipitation and wind. *Q. J. R. Meteorol. Soc.* **2016**, *142*, 2132–2142. [CrossRef]
79. Nguyen, P.; Shearer, E.J.; Tran, H.; Ombadi, M.; Hayatbini, N.; Palacios, T.; Huynh, P.; Braithwaite, D.; Updegraff, G.; Hsu, K.; et al. The CHRS Data Portal, an easily accessible public repository for PERSIANN global satellite precipitation data. *Sci. Data* **2019**, *6*, 180296. [CrossRef] [PubMed]
80. Funk, C.; Peterson, P.; Landsfeld, M.; Pedreros, D.; Verdin, J.; Shukla, S.; Husak, G.; Rowland, J.; Harrison, L.; Hoell, A.; et al. The climate hazards infrared precipitation with stations—A new environmental record for monitoring extremes. *Sci. Data* **2015**, *2*, 150066. [CrossRef] [PubMed]
81. Joyce, R.J.; Janowiak, J.E.; Arkin, P.A.; Xie, P. CMORPH: A method that produces global precipitation estimates from passive microwave and infrared data at high spatial and temporal resolution. *J. Hydrometeorol.* **2004**, *5*, 487–503. [CrossRef]
82. Prein, A.F.; Gobiet, A. Impacts of uncertainties in European gridded precipitation observations on regional climate analysis. *Int. J. Clim.* **2017**, *37*, 305–327. [CrossRef]
83. Bartsotas, N.S.; Anagnostou, E.N.; Nikolopoulos, E.I.; Kallos, G. Investigating satellite precipitation uncertainty over complex terrain. *J. Geophys. Res. Atmos.* **2018**, *123*, 5346–5359. [CrossRef]
84. Maggioni, V.; Meyers, P.C.; Robinson, M.D. A Review of Merged High-Resolution Satellite Precipitation Product Accuracy during the Tropical Rainfall Measuring Mission (TRMM) Era. *J. Hydrometeorol.* **2016**, *17*, 1101–1117. [CrossRef]
85. Sarachi, S.; Hsu, K.-L.; Sorooshian, S. A Statistical Model for the Uncertainty Analysis of Satellite Precipitation Products. *J. Hydrometeorol.* **2015**, *16*, 2101–2117. [CrossRef]
86. Tian, Y.; Peters-Lidard, C.D. A global map of uncertainties in satellite-based precipitation measurements. *Geophys. Res. Lett.* **2010**, *37*. [CrossRef]
87. Bowman, K.P. Four years of precipitation retrievals from the Tropical Rainfall Measuring Mission (TRMM) satellite are compared with data from 25 surface rain gauges on the National Oceanic and Atmospheric Administration/Pacific Marine Environment Laboratory (NOAA/PMEL'). *J. Clim.* **2005**, *18*, 178–190, ISSN 08948755. [CrossRef]

88. Gao, Y.C.; Liu, M.F. Evaluation of high-resolution satellite precipitation products using rain gauge observations over the Tibetan Plateau. *Hydrol. Earth Syst. Sci.* **2013**, *17*, 837–849. [CrossRef]
89. Rossi, M.; Kirschbaum, D.; Valigi, D.; Mondini, A.C.; Guzzetti, F. Comparison of Satellite Rainfall Estimates and Rain Gauge Measurements in Italy, and Impact on Landslide Modeling. *Climate* **2017**, *5*, 90. [CrossRef]
90. Adam, J.C.; Lettenmaier, D. Adjustment of global gridded precipitation for systematic bias. *J. Geophys. Res. Atmos.* **2003**, *108*, 4257–4272. [CrossRef]
91. Kochendorfer, J.; Nitu, R.; Wolff, M.; Mekis, E.; Rasmussen, R.; Baker, B.; Earle, M.E.; Reverdin, A.; Wong, K.; Smith, C.D.; et al. Analysis of single-Alter-shielded and unshielded measurements of mixed and solid precipitation from WMO-SPICE. *Hydrol. Earth Syst. Sci.* **2017**, *21*, 3525–3542. [CrossRef]
92. Kochendorfer, J.; Rasmussen, R.; Wolff, M.; Baker, B.; Hall, M.E.; Meyers, T.; Landolt, S.; Jachcik, A.; Isaksen, K.; Brækkan, R.; et al. The quantification and correction of wind-induced precipitation measurement errors. *Hydrol. Earth Syst. Sci.* **2017**, *21*, 1973–1989. [CrossRef]
93. Khodayar, S.; Davolio, S.; Di Girolamo, P.; Brossier, C.L.; Flaounas, E.; Fourrie, N.; Lee, K.-O.; Ricard, D.; Vie, B.; Bouttier, F.; et al. Overview towards improved understanding of the mechanisms leading to heavy precipitation in the western Mediterranean: Lessons learned from HyMeX. *Atmos. Chem. Phys.* **2021**, *21*, 17051–17078. [CrossRef]
94. Dayan, U.; Nissen, K.; Ulbrich, U. Review Article: Atmospheric conditions inducing extreme precipitation over the eastern and western Mediterranean. *Nat. Hazards Earth Syst. Sci.* **2015**, *15*, 2525–2544. [CrossRef]
95. Tramblay, Y.; Somot, S. Future evolution of extreme precipitation in the Mediterranean. *Clim. Chang.* **2018**, *151*, 289–302. [CrossRef]
96. Giorgi, F.; Raffaele, F.; Coppola, E. The response of precipitation characteristics to global warming from climate projections. *Earth Syst. Dyn.* **2019**, *10*, 73–89. [CrossRef]
97. Taylor, K.E. Summarizing multiple aspects of model performance in a single diagram. *J. Geophys. Res.* **2001**, *106*, 7183–7192. [CrossRef]
98. Varble, A.; Zipser, E.J.; Fridlind, A.M.; Zhu, P.; Ackerman, A.S.; Chaboureau, J.; Collis, S.; Fan, J.; Hill, A.; Shipway, B. Evaluation of cloud-resolving and limited area model intercomparison simulations using TWP-ICE observations: 1. Deep convective updraft properties. *J. Geophys. Res. Atmos.* **2014**, *119*, 13–891. [CrossRef]
99. Prein, A.F.; Rasmussen, R.M.; Wang, D.; Giangrande, S.E. Sensitivity of organized convective storms to model grid spacing in current and future climates. *Philos. Trans. R. Soc. Lond. Ser. A Math. Phys. Eng. Sci.* **2021**, *379*, 20190546. [CrossRef]
100. Roberts, N.M. *Stage 2 Report form the Storm-Scale Numerical Modelling Project*; Technical Report 407; MetOffice R&D: London, UK, 2003.
101. Petch, J.C. Sensitivity studies of developing convection in a cloud-resolving model. *Q. J. R. Meteorol. Soc.* **2006**, *132*, 345–358. [CrossRef]
102. Maulik, R.; San, O. A stable and scale-aware dynamic modeling framework for subgrid-scale parameterizations of two-dimensional turbulence. *Comput. Fluids* **2017**, *158*, 11–38. [CrossRef]